FACULDADE DE ENGENHARIA DA UNIVERSIDADE DO PORTO

Dual Active Bridge Converter for Electric Vehicle Charging

André Filipe Gama de Sousa Rodrigues

Mestrado em Engenharia Eletrotécnica e de Computadores

Supervisor: António José de Pina Martins

October 29, 2023

Abstract

Electric vehicles (EVs) are gaining popularity as a sustainable transportation option, but their widespread adoption is limited, due to the availability and efficiency of charging infrastructures, among other factors. There are different charging solutions, in particular with regard to electronic converters connected to the battery.

The dual active bridge (DAB) converter is a promising technology for EV charging, as it can operate at high power levels, offer high efficiency and due to its bidirectional characteristics. Therefore its understanding and evolution can be a key factor in expanding the market share of electric vehicles.

In this dissertation, a comprehensive study of the DAB converter for electric vehicle (EV) charging applications is presented, including its behavior, main characteristics, and type of control. A DAB prototype for EV charging will be designed and implemented to analyse its performance through simulation, and be further evaluated through experimental testing. The goal is to demonstrate the potential of DAB converters to enable efficient, powerful and reliable EV charging.

Resumo

Os veículos elétricos (EVs) estão a ganhar popularidade como uma opção de transporte sustentável, mas a sua adoção generalizada é limitada, sendo a disponibilidade e eficiência das infraestruturas de carregamento um dos fatores. Existem diversas soluções de carregamento, em particular no que respeita ao conversor eletrónico com ligação à bateria.

O conversor "dual active bridge" (DAB) é uma tecnologia promissora para o carregamento de veículos elétricos, pois pode operar em altos níveis de potência, oferecer grande eficiência e devido às suas caracteristicas bidirecionais. Portanto, o seu entendimento e evolução podem ser um fator chave na expansão da quota de mercado dos veículos elétricos.

Nesta dissertação, é apresentado um estudo abrangente do conversor DAB para aplicações de carregamento de veículos elétricos (EV), incluindo o seu comportamento, principais características e tipo de controlo. Também é projetado e implementado um conversor DAB para carregamento de veículos elétricos e é analisado o seu desempenho por meio de simulação. Além disso, é analizado o seu desempenho em protótipo por meio de testes experimentais verificando o seu comportamento com hardware. O objetivo será demonstrar o potencial dos conversores DAB para permitir um carregamento de veículos elétricos eficiente, potente e confiável.

Contents

List of Figures

List of Tables

Abbreviations and Symbols

AC	Alternating Current
DAB	Dual Active Bridge
DC	Direct Current
DPS	Double Phase Shift
EPS	Extended Phase Shift
ESS	Energy Storage System
EV	Electric Vehicle
G2V	Grid to Vehicle
IGBT	Insulated Gate Bipolar Transistor
MOSFET	Metal Oxide Semiconductor Field Effect Transistor
PHEV	Plug-in Hybrid Electric Vehicle
PWM	Pulse-Width Modulation
SoC	State of Charge
SPS	Single Phase Shift
TPS	Triple Phase Shift
V2G	Vehicle to Grid
ZVS	Zero Voltage Switching

i_L	Current in coil
I_o	Current output
P_o	Current input
V_o	Voltage output
V_p	Voltage in primary winding
V_s	Voltage in secondary winding
V_i	Voltage input
ϕ	Phase shift

Chapter 1

Introduction

1.1 Context and Motivation

Electric vehicles (EV) have emerged as a promising solution to mitigate the environmental impacts of transportation, reduce dependence on fossil fuels, and promote sustainable mobility. In the past few years, governments, manufacturers and consumers are increasingly embracing EVs as a viable alternative to internal combustion engine vehicles. However, despite the numerous benefits of electric vehicles, there are still some challenges and limitations that hinder their widespread adoption. Their limited amount of energy available, which is strictly dependent on the capacity of the vehicle's battery, affects the range of the EV and setbacks its use for long distance travel. Another hindrance is the limited availability of charging stations for public use, as the transition to widespread EV adoption is not solely dependent on the advancements in vehicle technology but also relies heavily on the development of robust charging infrastructure and charging technology.

The adoption of electric vehicles continues to grow and it is important to ensure that charging infrastructure is able to support the increasing demand for electricity and do so in a way that is efficient, reliable, and sustainable. To address these challenges, researchers and engineers are continuously exploring advanced charging technologies and power electronics solutions.

The Dual Active Bridge (DAB) converter is one such technology that has gained prominence in the field of EV charging due to it's bidirectional capability, among with its high power ratings and energy density, galvanic isolation and efficiency, and it is most commonly used in level 2 and level 3 charging stations.

1.2 Objectives

This dissertation takes a closer look at these charging stations, focusing on understanding the theory and functionalities of the DAB in the context of electric mobility. The theory is subsequently put into practice with software test simulations, emulating its role in a real DC fast charger, and

analysis of the waveforms and properties of some relevant variables produced at different conditions. Further tests are executed using hardware components for a "hands on" experience to analyse the working of the converter in real life situations in a scaled environment.

1.3 Structure

In addition to the introduction, this document is organised into five more chapters:

- Chapter 2 includes a review of the literature on the topic and an overview of the current state of the art in regards to electric vehicle charging and the converters that rival the DAB.
- Chapter 3 provides the necessary background information on the functionalities and main characteristics of the DAB converter.
- Chapter 4 details the PSIM simulation's implementation and results.
- Chapter 5 shows the experimental tests made, their results, the hardware that was used and explains the circuits built.
- Chapter 6 presents the conclusions drawn from the work completed and suggest some future works related to this one.

Chapter 2

State of the Art

2.1 World Electricity Production

When analysing data and studies from the global perspective of electricity production in the BP statistical review of world energy 2021, Figure 2.1, updated in January 2022, it appears that about 62% of global energy is generated by fossil fuels. Of the remaining percentage, 10% is generated by nuclear plants, 1% via other forms of fuel and leaving 28% created from renewable sources [10]. This shows that fossil fuels are still, nowadays, the main resource used in the production of electric energy in the world. As a type of non-renewable resource and due to its high demand, the continued reliance on fossil fuels is clearly unsustainable in the long term. This raises concern over the sustainable development of the world. However, this is just one of the main reasons that motivate the need to stop using these non-renewable resources. Other reasoning include the increase of pollution in the environment which this type of energy production promotes. A major problem of fossil fuels is the release of greenhouse gases during its combustion. These gases boosts the constant climate change in the terrestrial ecosystem, progressively and irreversibly destroying the planet.

To address the problems associated with fossil fuels, the world has increasingly focused on energy production through renewable energy sources. These types of sources use various natural phenomena to achieve a "greener" energy production, free from greenhouse gases, pollution and their consequences to the environment. As they are constantly present in nature, these resources are inexhaustible and thus promote the planets sustainable development. Various studies indicate that the production of energy by only using renewable sources, together with its efficient storage, can manage to suppress all the world's energy needs, with affordable prices, wide availability and with a clean and sustainable nature [11].

2.2 Electric Vehicle Shift and EV Charging Stations

The world emits each year approximately 50 billion tonnes of green house gases, and as seen in figure 2.2, 12% are due to road transportation [2]. These vehicles are constantly releasing

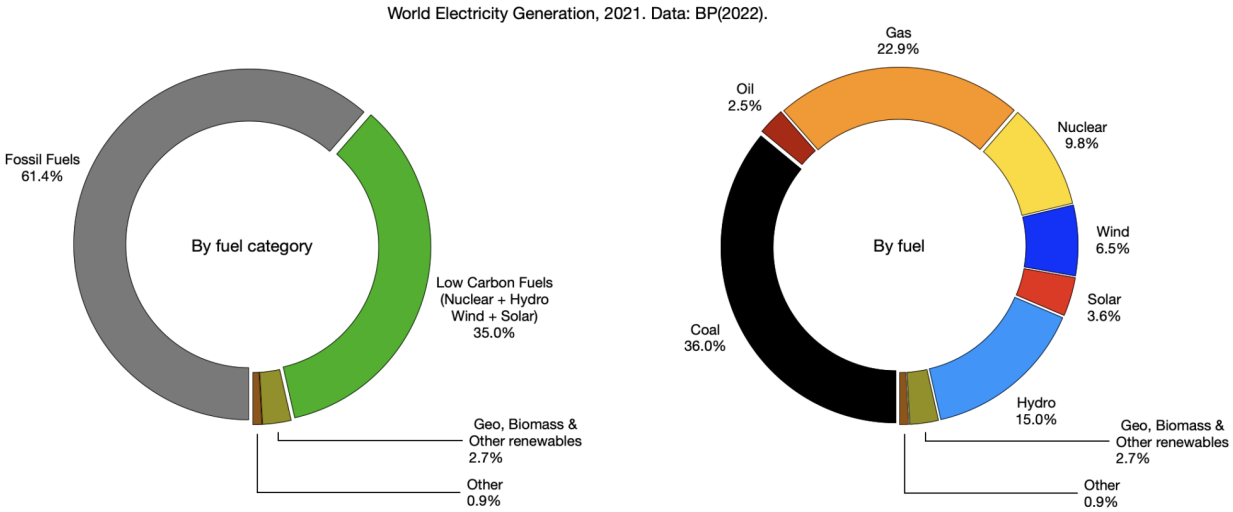

Figure 2.1: World electricity generation share in 2020 by fuel category and by fuel [1]. Data: BP Statistical Review of World Energy 2021

carbon dioxide (major component for green house gases) into the atmosphere and are responsible for around 25% of the total carbon dioxide emissions in the European Union [12]. This number explains the rise in rigidity of the world's commissions, in reaching carbon neutrality, in the so-called "decarbonisation" strategy by 2050 [13].

Due to all these factors, there is a huge push for the the replacement of combustion vehicles with electric vehicles [14]. Electric Vehicles, Hybrid Electric Vehicles and Plug-in Hybrid Electric Vehicles use electrical energy either as a primary fuel or to improve the efficiency of conventional combustion engines. They all use a battery, usually lithium, to store the electrical energy needed to power the engine. A very sudden spread of these vehicles is expected in the coming years, as their cost (purchase, use, maintenance, etc.) will become similar or better compared to cars with a combustion engine. This means that charging stations must develop at a rate at least equal to the rate of sales of these vehicles. Due to this fact and with the evolution of the Smart Grid, the storage of energy for later charging of these vehicles, through the Grid to Vehicle (G2V) technology, which is usually made up of a cascaded connection of an AC-DC and a DC-DC converter, is one of the most appreciated solutions. This technology allows the vehicle's battery to be in parallel with the electrical network during charging operations. However, it also allows the vehicle to supply energy to the grid like any other storage system (V2G mode), using bidirectional converters (power electronics) that guarantee an adequate strategy for managing the power flow.

2.2.1 AC vs DC charging

The power that is provided by the electric grid is always AC power, however, an electric vehicle, or any other electric component by that matter is only capable of storing DC power. This factor urges the power to be converted before storing it in the EV. There are two ways to charge the vehicle:

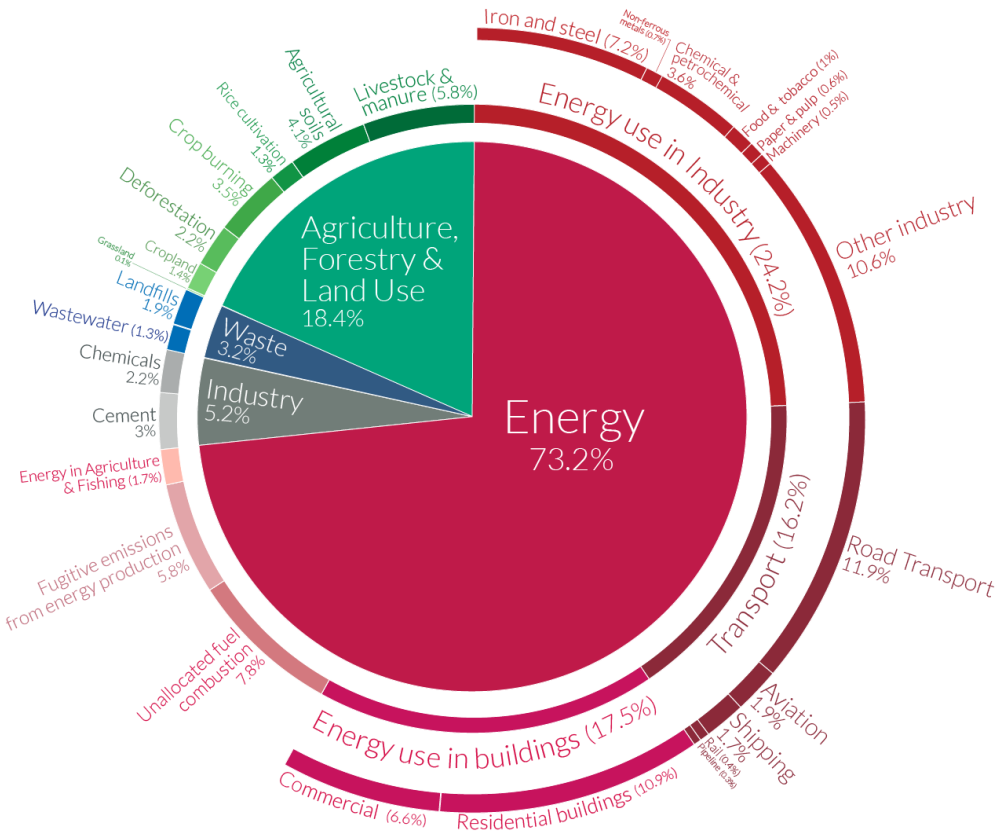

Figure 2.2: Global greenhouse gas emissions by sector [2]

AC and DC charging, each having their benefits and disadvantages and with its main difference being in the location of the conversion of power [3], in Figure 2.3 this difference can be observed.

In AC charging the power enters the car as AC, and it is only converted to DC in an onboard charger by an AC-DC converter that each EV possesses. These onboard chargers limits the amount of power converted, which makes the speed of charge of AC charging very time-consuming and much inferior in comparison to DC charging. In DC charging, or DC 'fast' charging as it is also referred, the DC power is directly passed to the battery, with no need for the onboard charger. This charger possesses converters with far greater efficiency and much more powerful, so that the car is delivered a big amount of power for the quickest possible time of charge. Although big power dump to the car may improve the charging time, its battery may be slightly damaged in comparisons to using AC charging in the long run, in recent studies on AC and DC chargers it was found that cars who used 'fast' charging more than three times a month would experience a 10% increase in battery degradation [3][15]. Due to this possible damage and to the different power threshold different EVs can withstand, each car has its own charging curve for DC fast charge. This curve will also affect the total charging time. The charging station is in constant communication with the EV and once this connection commences, the charger quickly reaches its maximum power output, however it is usual for an EV to only charge at it's maximum rate for a

fraction of the full charging period. After this, the power provided to the vehicle slowly decreases as the battery gets more charged, and when it reaches 80% a faster decrease of power starts. In Figure 2.4 it is shown a model of a common DC fast charge charging curve, with power output in the y-axis and SoC in the x-axis. A real charging curve is shown in Figure 2.5 which displays the charging curve of a Volkswagen model ID.4, which can withstand 130 kW on fast charge. This diagram shows the curve with a 50 kW charger in comparison to a 150 kW or greater charger.

Table 2.1 shows further differences between both charging types.

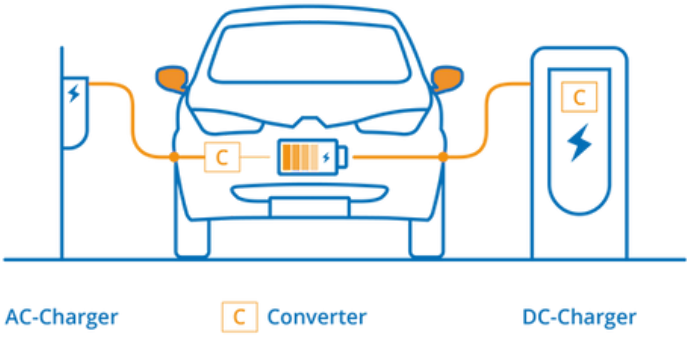

Figure 2.3: AC vs DC charging diagram. [3]

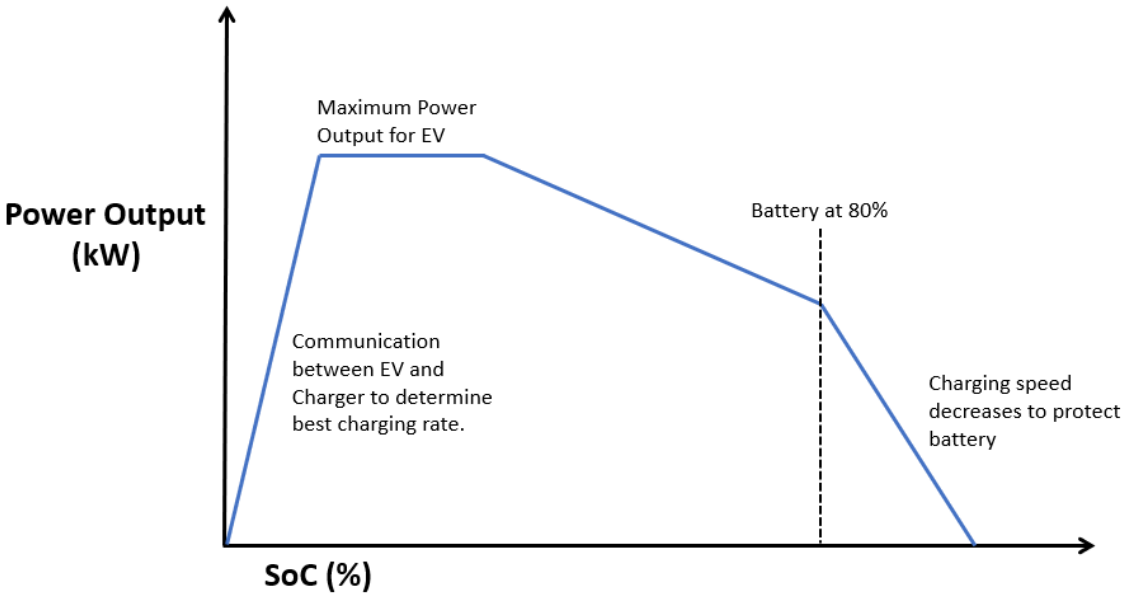

Figure 2.4: DC fast charge charging curve. Power output as y-axis and State of Charge (SoC) as x-axis. [3]

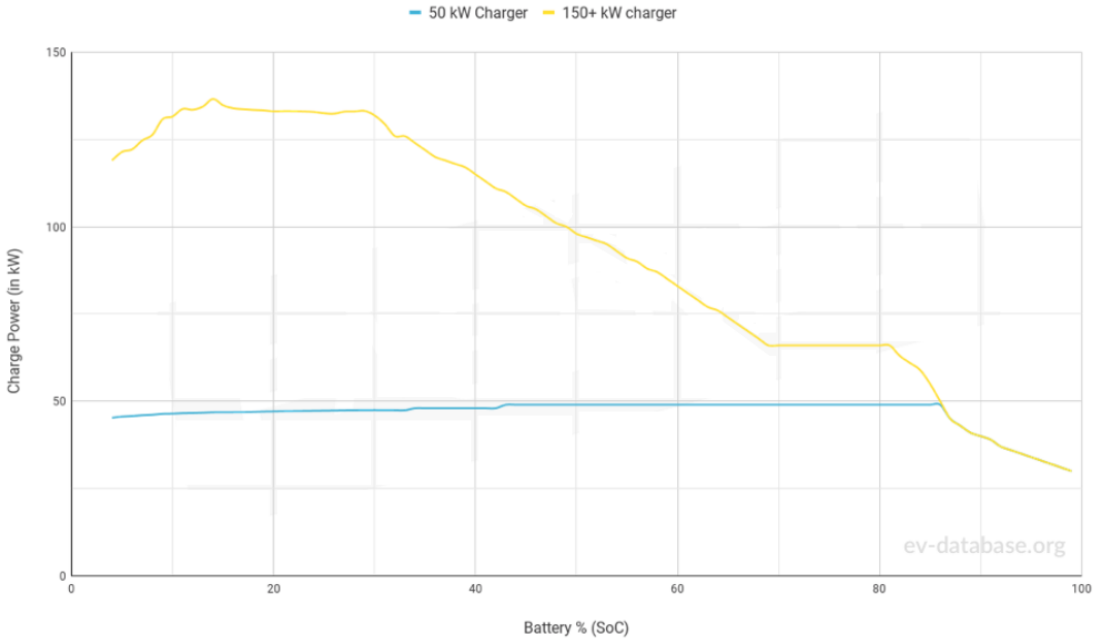

Figure 2.5: Comparison of Volkswagen ID.4 fast charging curve (150+ kW) with normal charging curve (50 kW) [4]

	AC charging	**DC charging**
Position of power converter	Onboard charger	Inside charging station
Speed of charge	Slower charging compared to DC	Faster charging
Placement of chargers	Common for house-holds and public charging	Only used for public charging
Charging curve	Constant line	Degrading charging curve
Electric battery	Safe for car battery	DC fast charge for a long time may degrade battery

Table 2.1: Differences between AC and DC charging.

2.2.2 Levels of EV charging

EV charging is also separated in three levels, these are used to differentiate the range of power output that is used to charge the car [16] [17].

- **Level 1:** The slowest charging level in terms of time, with an estimated charging time of between 22 hours up to 40 hours (estimation for an EV with a 40 kWh battery). It charges the car with AC power ranging between 1 kW to 1.8 kW.

- **Level 2:** Similar to the first level, Level 2 also charges the vehicle with AC power, however with a big increase in power output (3 kW - 22 kW), with the times of charging of a 40 kWh battery from 2 hours up to 13 hours.

- **Level 3:** The last level is also known as DC fast charging, and as it's name suggests it provides DC power to the vehicle. This level of charging is used for public charging, and the typical power output can go as high as 360 kW, which depending on the vehicle charge acceptance range the time of charge can be cut to only 15 minutes for a 40 kWh battery.

2.3 Vehicle-to-Grid Technology

A concept first put forward in 1997 [18], V2G consists on the ability for EVs to supply energy back to the electric grid, creating a bidirectional power flow between both [19].

EV batteries have the capability to store a substantial amount of power, and when parked (a car is parked for about 95% of their life span) could be perceived as a sizeable untapped energy storage device, and if used to its full potential could offer enormous benefits to the electric grid such as reactive power support, active power regulation, reducing electricity transport losses [20][21] and could benefit also our own household consumption. It is estimated that an average Portuguese family household consumes 275 kWh per month [22], dividing this number by 30 days gives a consumption per day of about 9 kWh, this means that an average EV car battery of 40 kWh could power a family home for about 4 days, a number that can be increased as these car batteries may even go to as high as 100 kWh.

Despite knowing this, using electric vehicles to support the electric grid is no simple task as there are structures that need to be put in place in order to fulfill it's bidirectional role. The smart grid must be able to support such system as well as EV charging stations and the vehicles itself must allow for the power to flow in either way. In regards to DC fast charging stations, the implementation of bidirectional DC-DC converters is a must. Figure 2.6 shows the interaction between DC-DC converters in EV charging stations and the smart grid. By interacting power sources and energy storage devices with the bidirectional feature, a reduction in size and cost as well as an increase in efficiency and performance of the system overall is reached as there is no need for two different converters to control each direction of flow [5].

2.4 Topology of Bidirectional DC-DC Converters

Bidirectional DC-DC converters can be divided between isolated and non-isolated, these categories mainly diverge, as the name refers, in their isolation. Non-isolated converters have no magnetic isolation when transferring the power as they do not use transformers. This topology is simpler to arrange, lighter and do not experience magnetic interference. Isolated converters on the other hand, convert the DC voltage input to AC and then rectify them back to DC, passing through a high frequency transformer between the second conversion. This topology has a significant voltage gain in comparison to the non-isolated and are much better suited to fast-charging stations due to this [5].

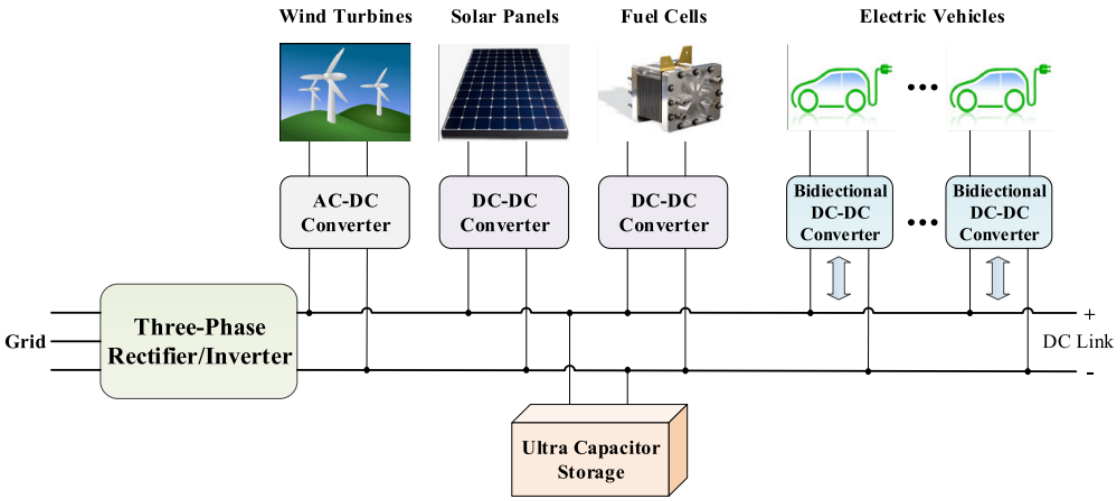

Figure 2.6: Diagram of bidirectional EV charging stations in grid [5]

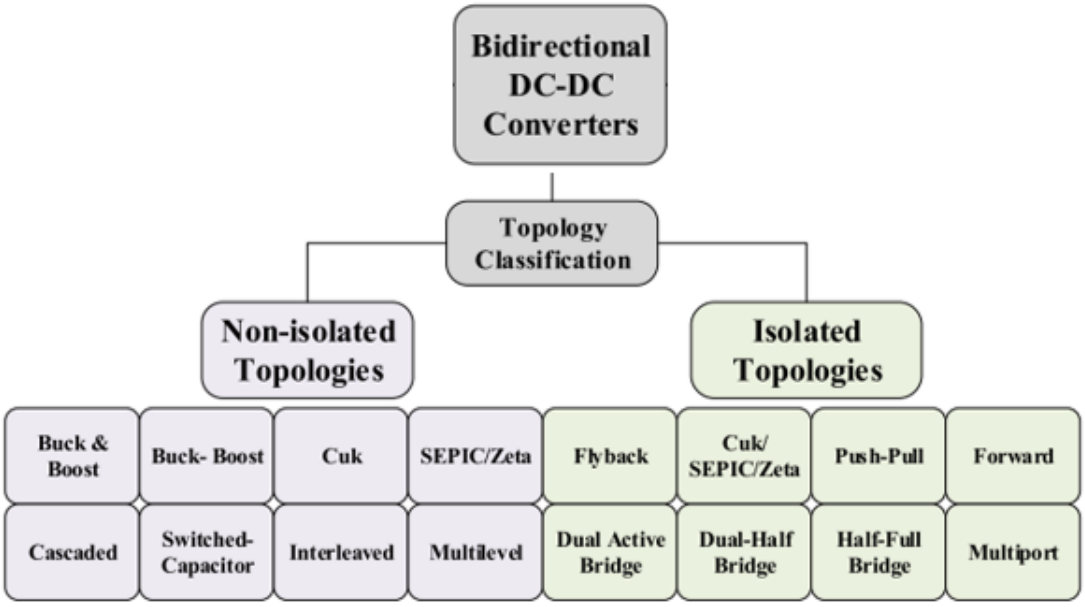

Figure 2.7: DC-DC topology flowchart [5]

2.4.1 Isolated Converters

Isolated bidirectional converters are the main option employed for air crafts, renewable energy sources and electric vehicle charging, its galvanic isolation bring high gain ability as a consequence of the turn ratio of the windings, making it appropriate for a wide range of input voltage and load regulation [23]. The isolation will also facilitate the possibility of various input and/or output topologies and are much better suited to high power application when comparing to non-isolated converters. It's isolation also provides a greater safety element for the equipment.

The Dual Active Bridge (which will be further explored in Chapter 3) fits in to this category, and some of the main isolated DC-DC converter topologies that compare to it will be briefly explored below.

2.4.1.1 Bidirectional Flyback Converter

Also know as the isolated Buck-Boost bidirectional converter, it is implemented, as seen in Figure 2.8, by switching the inductor of a Buck-Boost converter with a transformer for galvanic isolation. The transformer design is extremely important and a voltage clamp snubber is required for current leakage protection.

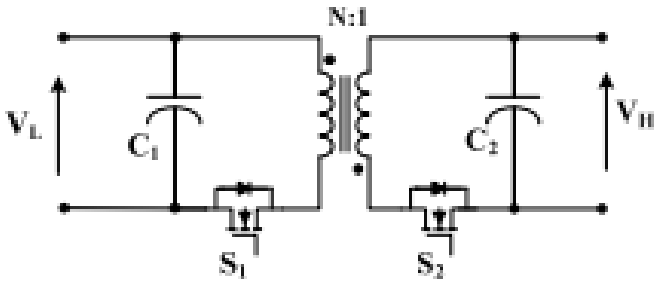

Figure 2.8: Bidirectional Flyback DC-DC Converter [5]

2.4.1.2 Isolated Cuk & Sepic/Zeta Bidirectional Converter

Made to introduce the benefits of magnetic isolation to the original Cuk converter. Figure 2.9 shows the converters layout, providing isolation between both input and output sides with high voltage gain. A useful feature this converter possesses for renewable energy systems is the coupling of the input and output inductors leads to the elimination of current ripples [24].

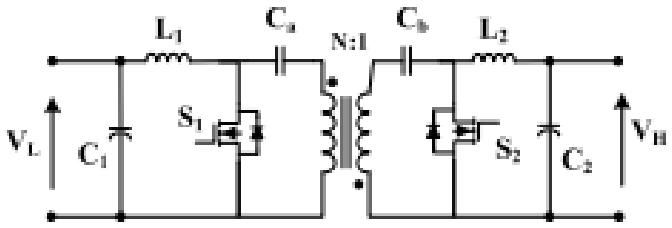

Figure 2.9: Isolated Cuk & Sepic/Zeta Bidirectional DC-DC Converter [5]

2.4.1.3 Push-Pull Bidirectional Converter

The circuit in Figure 2.10 was created to allow bidirectional flow on the original push-pull converter; it converts the power using a multi-winding transformer. For high power applications a three-phase bidirectional push-pull converter is proposed.

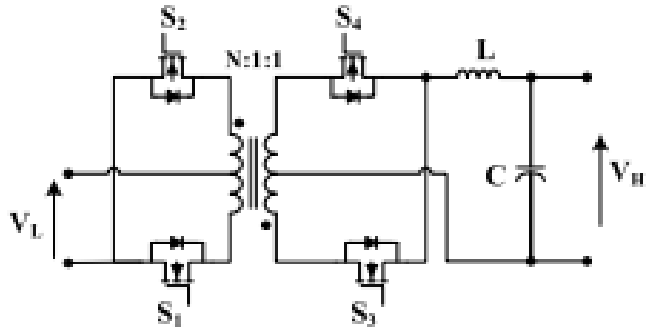

Figure 2.10: Push-Pull Bidirectional DC-DC Converter [5]

2.4.1.4 Forward Bidirectional Converter

A bidirectional model of the normal forward converter. This converter achieves zero voltage switching when a clamped circuit is used. This topology also brings about several hybrid configurations with the other isolated topologies mentioned.

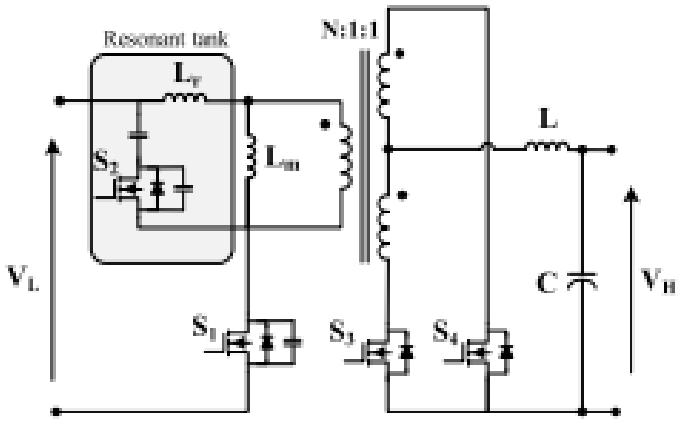

Figure 2.11: Forward Bidirectional DC-DC Converter [5]

2.4.1.5 Dual Half-Bridge Bidirectional Converter

An alternative to the DAB converter (the converter focused on this dissertation and seen more in depth in the next chapter), the Dual Half-Bridge, Figure 2.12, is used for applications with lower

power, having the number of power switches reduced from eight to four, and using two voltage-fed half-bridges in either sides. This converter may also be configured with a current-fed topology in the secondary side, which enables continuous current waveform.

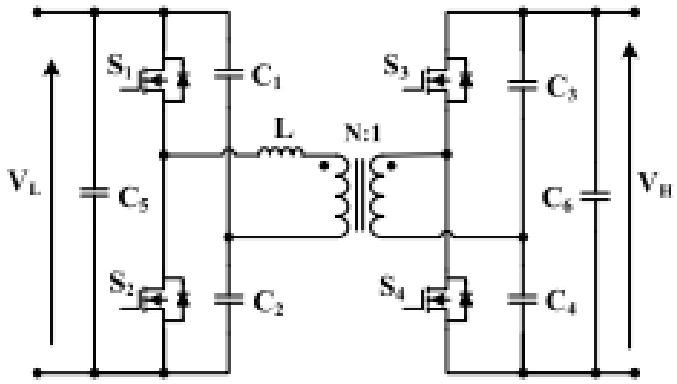

Figure 2.12: Dual Half-Bridge Bidirectional DC-DC Converter [5]

2.4.1.6 Half Bridge-Full Bridge Bidirectional Converter

Figure 2.13 shows the Half Bridge-Full Bridge Converter: it is composed by a voltage-fed half-bridge and full-bridge topology in the primary and secondary sides, respectively. Its lower count of switches makes for a simpler control in comparison to the DAB. This converter is useful for UPS topology integration.

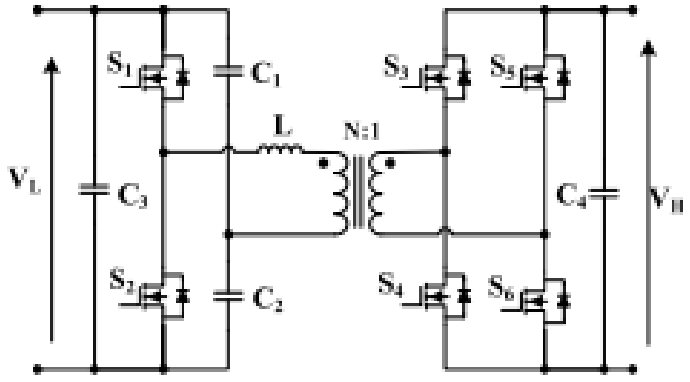

Figure 2.13: Half Bridge-Full Bridge Bidirectional DC-DC Converter [5]

2.4.2 Control Schemes for Bidirectional Converters

A big factor to extract the maximum efficiency of a converter is the correct choice of control schemes, and there are numerous possibilities for bidirectional DC-DC converters. Nevertheless

the main control schemes utilized for bidirectional DC-DC converters in electric vehicle applications are usually the PI, PID, sliding mode, Fuzzy and Digital control.

The PID and PI control is highly regarded due to its simple implementation, it relies on a control loop feedback system that receives a reference value set for its desired output, which is subtracted to the current output to give an error component, this error will be adjusted and tuned according to the three parts of the PID: Proportional; Integral and Derivative components, for the PI controller, only the Proportional and Integral parts are used for the calculation. These control techniques are extremely effective when it comes to the managing the power flow in both directions. Figure 2.14 shows the PID system diagram.

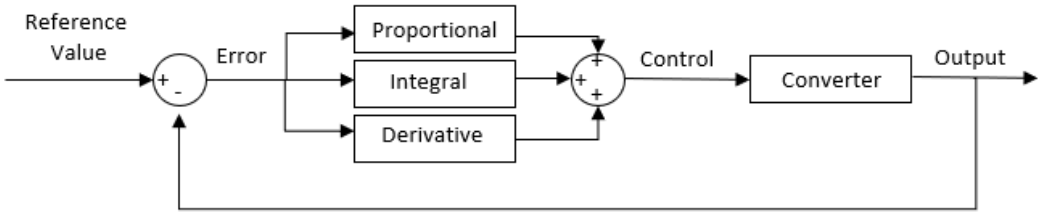

Figure 2.14: PID control feedback diagram

The PI control will be further explored on PSIM software simulations thought the dissertation. Document [25] shows a robust design of the PI control, exploring it's advantages and limitations.

For the sliding mode control, which its feedback diagram can be observed in Figure 2.15, it's objective is to alter the dynamics of a non-linear system and to stabilize it with uncertainties and disturbances. To do so, it defines a sliding surface in the state space, and a control law is designed to drive the system's trajectory onto this surface, keeping it there. The control law includes reaching control, which attracts the system toward the sliding surface, and sliding control, which drives the system along the surface towards the desired equilibrium point. The key concept behind sliding mode control lies in the Lyapunov stability theory, which is used to analyze the stability properties of the sliding surface, ensuring that the system's state trajectory converges to the sliding surface and remains on it despite the aforementioned uncertainties and disturbances.

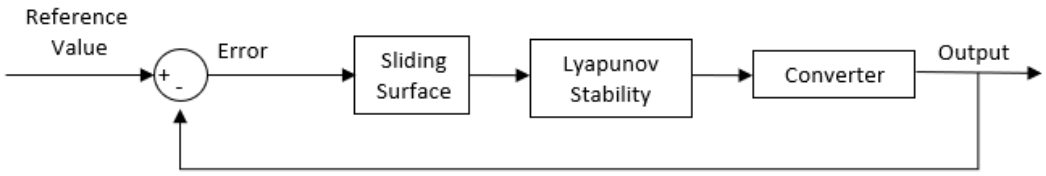

Figure 2.15: Sliding mode control feedback diagram

Fuzzy control is a dynamic and adaptive control technique used in DC-DC converters to regulate their operation. Unlike traditional control methods, fuzzy control doesn't rely on precise mathematical models. Instead, it uses linguistic variables and rules to handle the converter's complex and nonlinear behavior, defining fuzzy sets for input and output variables. Based on these linguistic variables and rules, the fuzzy controller makes decisions and adapts the control action accordingly. Fuzzy control effectively handles uncertainties, parameter variations, and disturbances commonly encountered in DC-DC converters. By employing fuzzy logic, the control action can be fine-tuned to optimize efficiency, maintain stable power conversion, and ensure reliable performance under varying operational conditions.

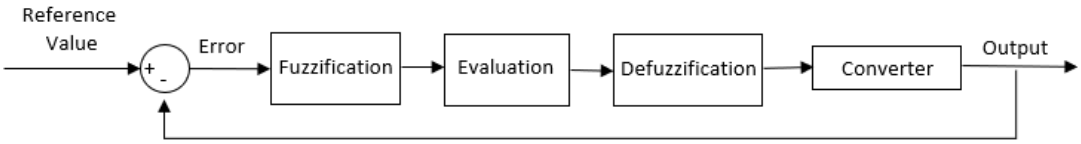

Figure 2.16: Fuzzy control feedback diagram

Document [26] analyses the fuzzy control and sliding mode control on the DAB converter for battery charge and discharge applications. For the fuzzy control, less measurements and no prior knowledge are needed for its design. The sliding mode offers a faster converging and more robust control.

In digital control systems, continuous-time error signals are first converted into a digital format that can be processed by a computer, using an Analog-to-Digital (A/D) interface. Once the error signal is in digital form, it undergoes processing within the computer, which is then fed to a controller, and the controller's output injected into the system, which in this case is the converter. This way, the digital controller can efficiently and precisely regulate the system's behavior based on the processed error signal, enabling precise and responsive control of the converter's operation. The feedback diagram of this control scheme is seen in Figure 2.17.

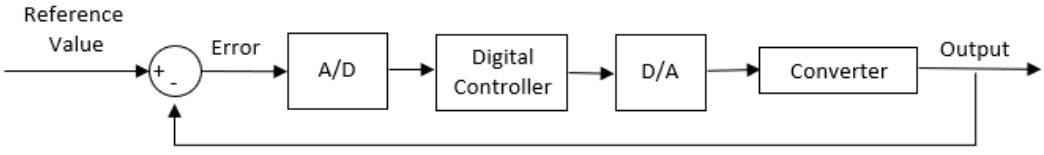

Figure 2.17: Digital control feedback diagram

For a precise small-signal model of a DAB converter, a thorough understanding of the modulation method and the inclusion of electromagnetic interference (EMI) filters, accounting for their interactions with the DAB, are essential, as analysed in the article [27]. High-power converters are increasingly relying on the use of Digital Signal Processors due to their cost-effective high computational performance. Digital implementation offers a greater flexibility compared to analog electronics, high immunity to electromagnetic interference, and the ability to monitor processes and faults using external interfaces or network connections. Hence, a digital control platform was employed to regulate the article's DAB, and the discrete-time transfer function derived from discrete modeling, readily utilized for designing the controller.

Table 2.2 shows the benefits and limitations of the four control schemes suggested.

Control Scheme	**Control Problems**	**Benefits**	**Limitations**
PID	-Power flow control -Minimizing switching time between two directions -Reducing dead time of switches -Protecting the elements from over current	-Low cost -High reliability -High dynamic performance	-Low efficiency -Lack of robustness with uncertainties and disturbances -Weakness in avoiding large transient between directions
Sliding Mode	-Considering external perturbations in large signal -Dealing with severe variations in load and line	-Reference tracking -Fast and finite-time response -Robustness against parameter variation and external perturbation -Ability to characterise the system under small and large conditions	-Accurate parameter and state information are needed
Fuzzy	-Minimizing power consumption from the grid -Attaining smooth performance of super-capacitor in charge/discharge -Minimizing control time	-Fast and robust response -Applicability to nonlinear and inaccurate systems	-Sensitive to expert knowledge
Digital Control	-Accurate small-signal modelling of DAB -Changing power flow directions smoothly with current protection -Improving the transient response's speed	-High EMI immunity -Enhances the efficiency and charge/discharge speed -Higher flexibility -Fault monitoring -Ease of use -Improved reliability	-Difficult to implement the electronic configuration of nonlinear control law -Requiring great analog/digital processing effort

Table 2.2: Summary of control schemes in bidirectional converter [5]

Chapter 3

Background on the Dual Active Bridge

The DAB converter is one of the favoured bidirectional isolated converters, it consists of a high frequency transformer in between two full H-bridges. This converter is gaining traction among Micro grids and Electric Storage Systems, not only for its bidirectional adjustable power flow capabilities but also for its simple structure, high power density, wide voltage conversion gain range and soft switching features [28]. It's high switch count (eight power switches), accompanying the galvanic isolation in this topology makes it an adequate fit for high power applications [29] such as DC fast charge for EVs. For these applications the DAB is employed to regulate the DC voltage supplied to the vehicle from the three-phase rectifier. In the following sections the theoretical concepts of the DAB's operating system with a PI controller and Single Phase Shift will be explained.

3.1 Theoretical Development

Figure 3.1 shows a circuit diagram of the DAB, as touched previously, it consists of a high-frequency transformer and connects two similar H-bridges made up with transistors, the first one being a DC-AC inverter and the second being a AC-DC inverter, together making a full DC-DC converter. It allows the control of power flow in the circuit depending on the phase shift between the square waves (V_p and V_s) applied to the bridges (Single Phase Shift), and will affect the MOSFET or transistor pair that is conducting simultaneously making a total of 4 different operating modes. Observing the waves on Figure 3.2 and the Table 3.1 along with Figure 3.3, we can verify the change of the current wave in the coil (i_L) at each mode of operation and what each operating mode means in regards to the conducting components.

The difference applied in the angle ϕ, will affect the waveform current in the coil and, consequently, the average current in the output which will be a rectified (i_L) wave. These changes will impact the output power to the battery.

When working with the Dual Active Bridge, the maximum power flow is obtained when the offset angle ϕ between the waves is equal to $\pi/2$ rad as it obtains the highest possible average current. When the secondary wave is lagging behind the primary, a flow of current will be directed

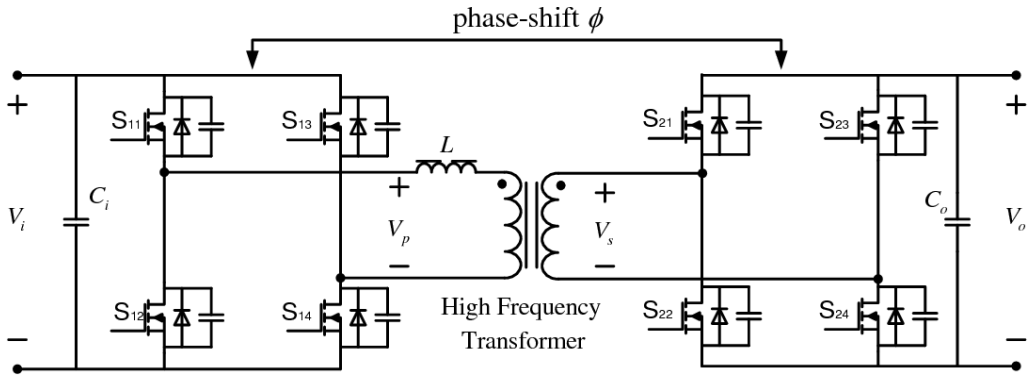

Figure 3.1: DAB converter circuit [6]

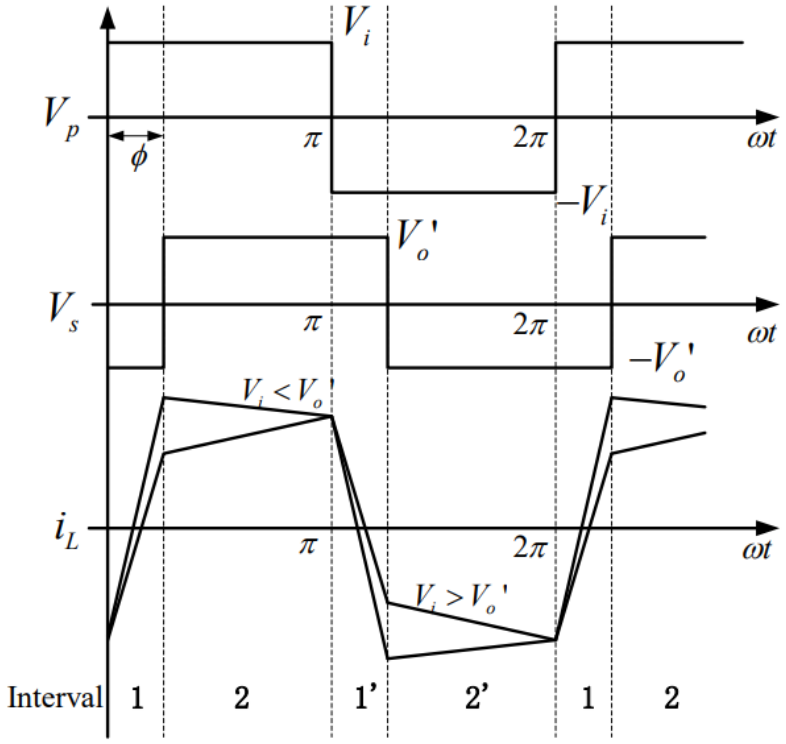

Figure 3.2: DAB waveforms for forward power flow: Primary Voltage, Secondary Voltage and Coil Current respectively [6]

Table 3.1: Operating modes of the DAB

Operating Modes	Transistor Pairs Conducting
1	S11, S14 & S22, S23
2	S11, S14 & S21, S24
1'	S12, S13 & S21, S24
2'	S12, S13 & S22, S23

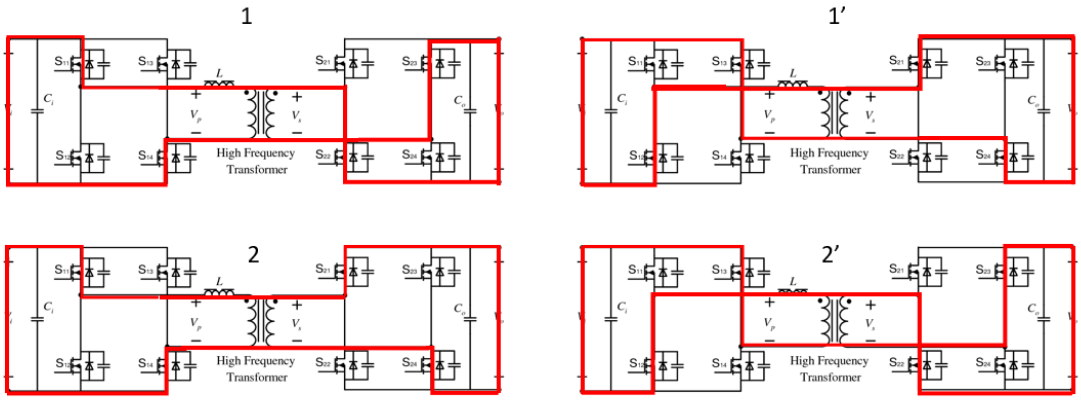

Figure 3.3: DAB Current flow at each operating mode.

from the primary to the secondary side, and conversely, when the primary wave is lagging behind the secondary, the direction of the current flow will be reversed, bringing about its bidirectional feature. This versatility in power flow direction is one of the key advantages of the DAB converter in V2G operations.

3.2 Design

The design of the DAB is critical for its performance, and requires careful considerations of various factors.

The DAB operates at high frequencies, enabling smaller and more efficient components, one of which is the transformer. For the transformer design, it is extremely important to decide its turn ratio, $n = V_s/V_p$. There is a possibility of adjusting the wave to a boost ($V_p > V_s/n$), buck ($V_p < V_s/n$) (both of them can be seen in the i_L wave on Figure 3.2), or ideally equalling V_s/n to V_p. This ideal scenario would help the efficiency of the DAB by reducing the rms current and reactive power.

During the DAB design it is also important to consider its peak power operating conditions. As addressed previously, the current, and consequently the power, would be adjusted by the angle ϕ, ranging on the values [-π/2, π/2], however, despite the maximum possible power flow being at these two points, its range should be decreased, as the power flow flips at these angles, from positive flow to negative, and to allow room for transients. At maximum power, the maximum angle should be close to, but not equal to π/2.

Regarding the size of the coil, it is important to inspect the equations for a Dual Active Bridge, which, with a deduction of the area within the output current wave we will be able to arrive at the equations 3.1 and 3.2 for the output current and power respectively.

$$I_o = \frac{V_i \phi (1 - \phi/\pi)}{2n\pi F_s L} \tag{3.1}$$

$$P_o = V_o I_o = \frac{V_o V_i \phi (1 - \phi/\pi)}{2n\pi F_s L} \tag{3.2}$$

With these equations we can verify that the size of the coil is essential to maximise the power extraction, as the bigger the coil, the smaller the maximum power. By modifying the expression 3.2 as a function of the coil (L), we can calculate its size for the power needed.

3.3 Control

For the circuit control, it is important to decide which control scheme to use and how to handle the transistor switching. There are many different variations that can be opted for both these operations, with each having positive and negative characteristics.

For the choice of control scheme the variations explored in Chapter 2.4.2 for bidirectional DC-DC converters are all suitable for DAB applications, with the PI controller being chosen to further explore the DAB with PSIM software testing.

For the PI controller, its main objective is to control the current by establishing a reference value for the power wanted, and comparing it to the exact value measured on the output, and altering the angle of phase shift ϕ according to its proportional and integral components. Figure 3.4 shows the working diagram theory for a PI controller working on the DAB converter.

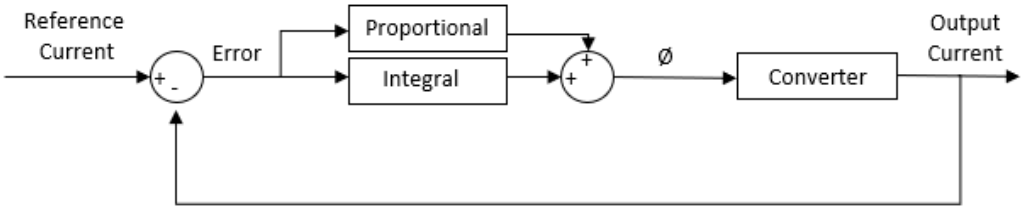

Figure 3.4: PI controller diagram for DAB applications

As for the switching strategy, the aim is to maximize power range and optimize ZVS characteristics. There are four usual switching strategies for the DAB: Extended phase shift (EPS), Double phase shift (DPS), Triple phase shift (TPS) and the one most prominent in this thesis the Single phase shift (SPS) [7].

Single Phase Shift concept is the more traditional route when it comes to controlling the DAB, and has already been touched on in the theoretical development section. In comparison to the SPS which relies on one phase difference between the primary and secondary sides, the EPS control adds an equal inward shift between the primary and the secondary side on the basis of SPS and

the DPS adds an inward shift in both at the same time [7], their respective waves can be seen in Figure 3.5 and can be compared to the single phase shift waves in Figure 3.2.

3.4 Interleaved Dual Active Bridge

The Interleaved DAB converter (which can be seen simulated in Figure 4.2) is a sophisticated power electronics topology that combines the benefits of both the Dual Active Bridge and interleaving techniques, and has its main ability in efficiently managing high-power conversions. It consists of multiple identical dual active bridge converters connected in parallel.

The purpose of interleaving is to improve the overall performance and efficiency of the system. By splitting the power among multiple parallel-operated bridges, the interleaved dual active bridge converter reduces the current and voltage stress on each converter, resulting in various advantages, for instance: reduced device stress, as it allows the distribution of power across several power semiconductor devices, leading to lower current and voltage ratings on each device, extending the converter's lifespan and increasing reliability; reduced switching losses, as it reduces the switching frequency seen by each bridge, thereby lowering switching losses; reduced output ripple, among other benefits [30].

This variation of the DAB can mitigate the challenges associated with high currents and voltages, leading to improved efficiency, reduced stress on components, and enhanced power handling capabilities.

3.5 Conclusions

This chapter presented the theory behind the workings of the DAB converter, how it functions and it's waveforms. It was understood it's design and important parameters to set to obtain expected results. This section demonstrated the DAB converters flexibility in regards to adjusting power flow in not only one direction but in both, and it's great response to different power levels, exhibiting it's amazing potential for EV fast charging station.

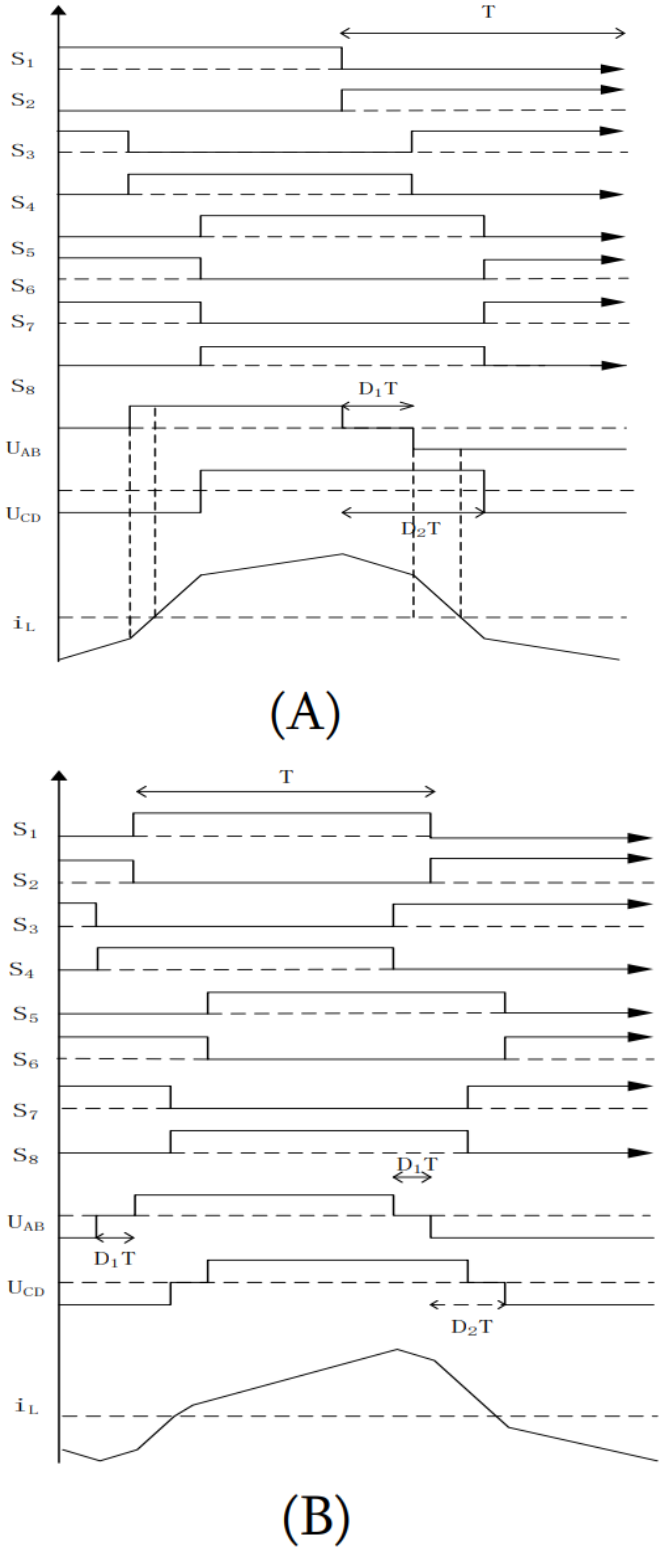

Figure 3.5: Waveforms for (A) EPS and (B) DPS [7]

Chapter 4

Simulation Test

To confirm the validity of the theoretical research, a set of simulations werw conducted using the PSIM software. PSIM (Power System Simulation for Industrial Motors) is a simulation software used to analyse and design electrical power systems. It is commonly used in the fields of electrical engineering and power electronics to model, simulate, and test power system components. The aim is to simulate a Dual Active Bridge converter working in a DC fast charger for electric vehicles, observing the behaviour of the power system under different operating conditions and test its performance before implementing a scaled model of the DAB in the experimental phase.

4.1 Objective

The objective of this simulation was to emulate a Dual Active Bridge converter working in a 100 kW DC fast charging station, charging a Volkswagen ID.4 battery system according to its fast charging curve in Figure 2.5, and subsequently analysing and interpreting appropriate waveforms to validate its correct implementation. Further simulations were made with an interleaved DAB to highlight its additional properties.

4.2 Specifications and Circuit Setup

The simulation was set up according to the specific requirements of EV charging in real-life situations, and the DAB components were designed based on the previously studied theory. Table 4.1 shows the specifications made for the simulation.

Table 4.1: Simulation value table.

V_i	650 V
V_{omin}	300 V
V_{omax}	400 V
$V_{o80\%SoC}$	380 V
n	0.5
P_{omax}	100 kW
ϕ	$-\pi/6, 2\pi/5$
L	$26.5\mu H$
fs	20 kHz

The voltage V_i entering the DAB was chosen from a realistic value for an EV charger, it simulates the DC voltage arriving from the AC-DC converter that is connected to the public 3-phase grid, and is usually around 650 V for a direct connection to the grid.

Voltage on the battery was considered on the basis of the battery specifications of the VW ID.4 model [4]. It was calculated by multiplying the voltage value of a fully charged lithium cell (4.2 V) by 96 the number of cells in series in the vehicles battery, this would give 400 V maximum output voltage to the battery. It's model was based on a Thevenin circuit equivalent model for an EV battery [31].

The switching frequency was predetermined to be 20 kHz, as the DAB functions with high frequencies, and finally ϕ was chosen to be a little below its maximum possible quantity for their to be a safe distance in angle before a full power direction switch occurs, the choice of maximum ϕ value was made by subtracting 0.1π from the 0.5π that set the maximum power flow. The bidirectional capability angle ϕ was limited to a minimum of negative 30 degrees.

The next components were calculated with the theory gathered. Value n for the turn ratio in the transformer uses the known equation $n = V_o/V_i$, V_i and V_o depends on the state of charge of the battery, so to minimize the reactive power, V_o was set at approximately the middle point between maximum charging voltage (with car at 80% SoC) and minimum V_o. The coil was chosen by adapting the equation 3.2 and substituting all the other known variables.

To simulate the DAB in conditions closer to real life, IGBT values where chosen according to suitable transistors on the market. The respective values to fill would be the saturation voltage, transistor resistance, diode forward voltage and diode resistance. After analysing several IGBT datasheets, the model chosen for the transistors in the first bridge would be the Infineon FF300R12KS4 model. This transistor has a nominal voltage capacity of up until 1200 V and nominal current until 300 A, which is within the limitations for the first bridge. By looking at the datasheet [32], we can find it's saturation voltage of 3.2 V and diode forward voltage of 2 V, to calculate the transistor and diode resistance we would need to find the value for the maximum current rating in the datasheet which would be at 400 A, by dividing the saturation voltage by the maximum current rating we would obtain the transistor resistance (0,008 Ω) and by dividing the diode resistance by the same maximum current rating we obtain the diode resistance (0.005 Ω). For the second bridge the voltage would be halved due to the transformer, however higher

current levels would pass through the transistors. The IGBT model Infineon FF400R06KE3 was chosen, with a nominal voltage of 400 V and a nominal current of 600 A, it would be well within the maximum power output possible. By analysing it's datasheet [33], and using the same process carried out for the first IGBT model the values found where: Saturation Voltage = 1.45 V; Diode Forward Voltage = 1.55 V; Maximum current rating = 500 A; Transistor Resistance = 0.0029 Ω and Diode Resistance = 0.0031 Ω.

With these specifications the circuit seen in figure 4.1 was built, and for further testing Figure 4.2 shows the circuit for the interleaved DAB.

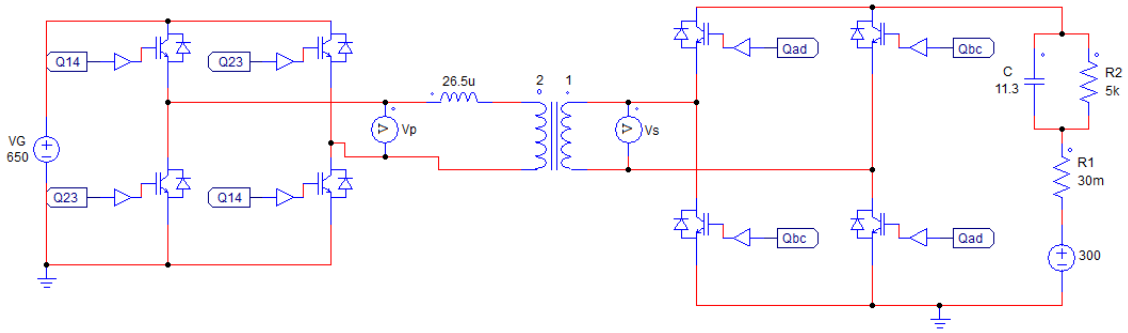

Figure 4.1: DAB circuit on PSIM.

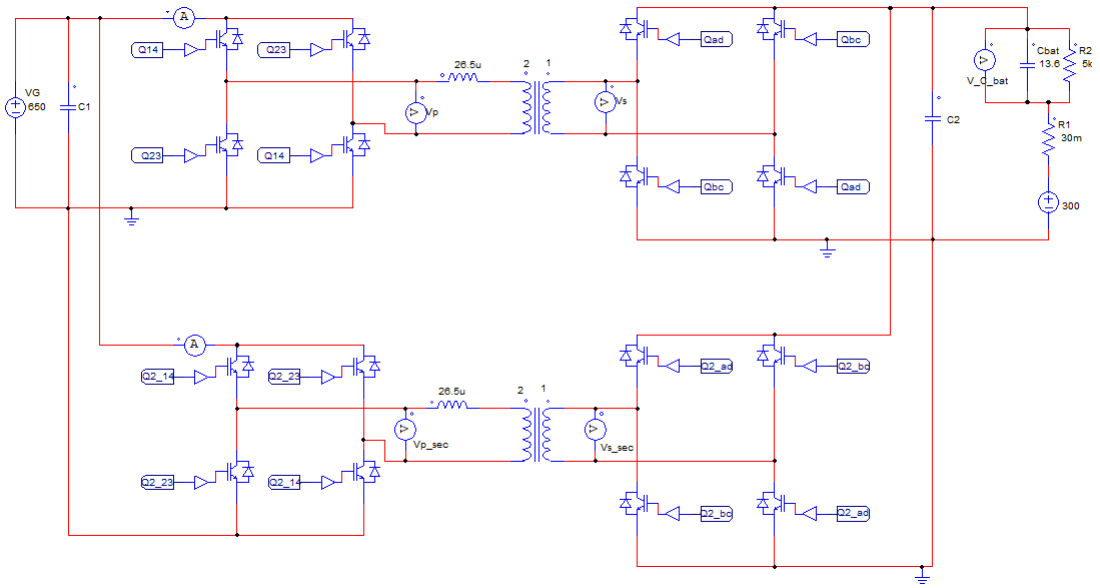

Figure 4.2: Interleaved DAB circuit on PSIM.

4.3 Control

4.3.1 Phase Shift Control Implementation

On figure 4.3 it can be observed the control signal used for the Single Phase Shift of the DAB, implemented to the IGBT pairing. A sawtooth wave was used in the primary and secondary bridge pairings, with the second bridge having a reference angle (phi) in degrees, multiplied by -1 that would determine the phase shift. The respective outputs would then pass through a sine component, which produces two sine waves shifted by the reference angle set, and when comparing it with the neutral creates a PWM control with the shift applied on the second bridge. As discussed earlier this shift is crucial for the DAB converter.

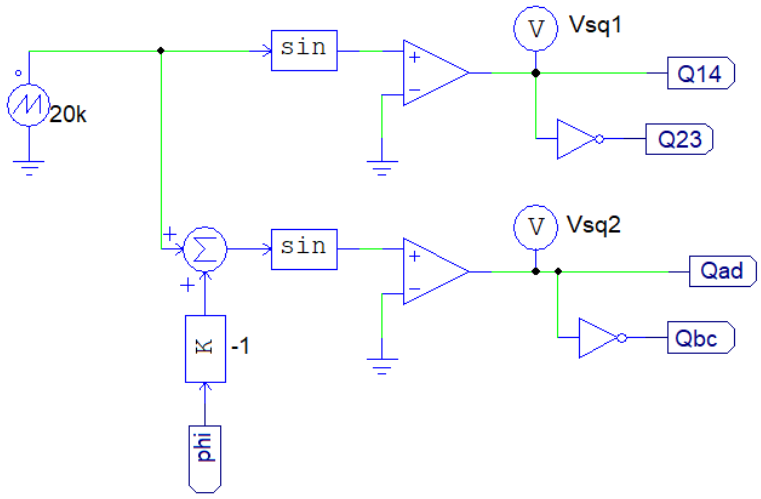

Figure 4.3: Phase shift control Circuit on PSIM.

Figure 4.4 shows the step by step waveform transformation until the final phase shifted waves. 1) Sawtooth and Sawtooth with shift; 2) Shifted sine waves; 3) Final phase shifted waves;

The interleaved phase shift control was carried out as per the theory suggested, similarly to the simple DAB, the square waves for the first DAB component of the interleaved model where formed with a sawtooth and a sine comparison to the neutral with the secondary bridge being shifted "phi" degrees. For the second DAB component, the whole system was lagged 90 degrees before building the square waves. Figure 4.5 shows the phase shift control constructed, and Figure 4.6 shows the square waves with a phase shift of 30 degrees; Note that on the second graph of this figure the waves are lagging 90 degrees in comparison to the first.

4.3.2 PI controller

To establish the PI controller, based on the one seen on Figure 4.4, first the charging curve for the desired power output (P_ch) was built in a code block, and was divided by the filtered Voltage output of the converter, to obtain the reference current. To this reference, the filtered output current

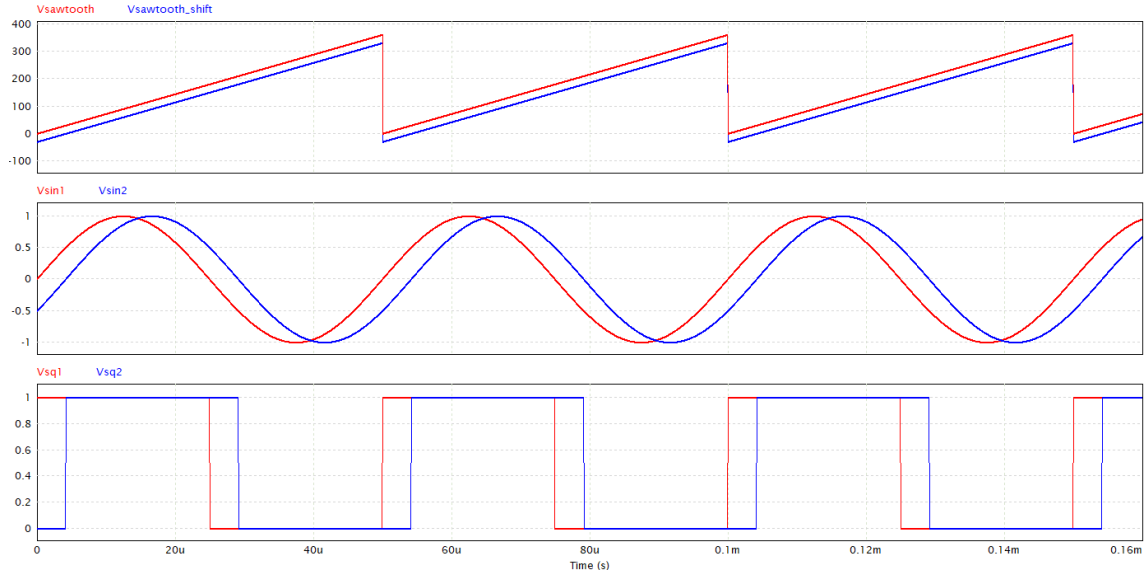

Figure 4.4: Phase shifted PWM wave built step by step.

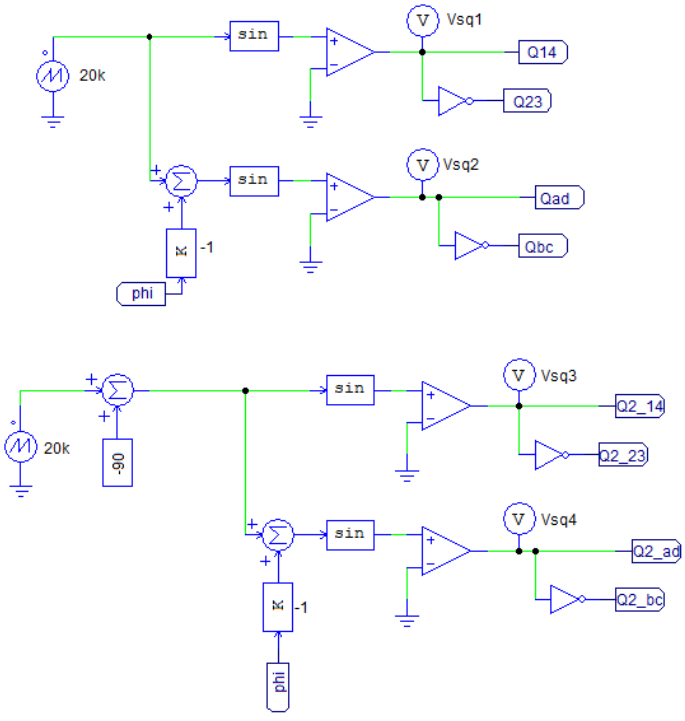

Figure 4.5: Phase shift control circuit for interleaved DAB on PSIM.

would be subtracted to receive the error value of the system. The PI function block would then transform the error in to the angle phi which would be inserted as the phase shift on the PWM transistor waves.

The charging curve was loosely based around the one seen on Figure 2.5. Its functioning plan

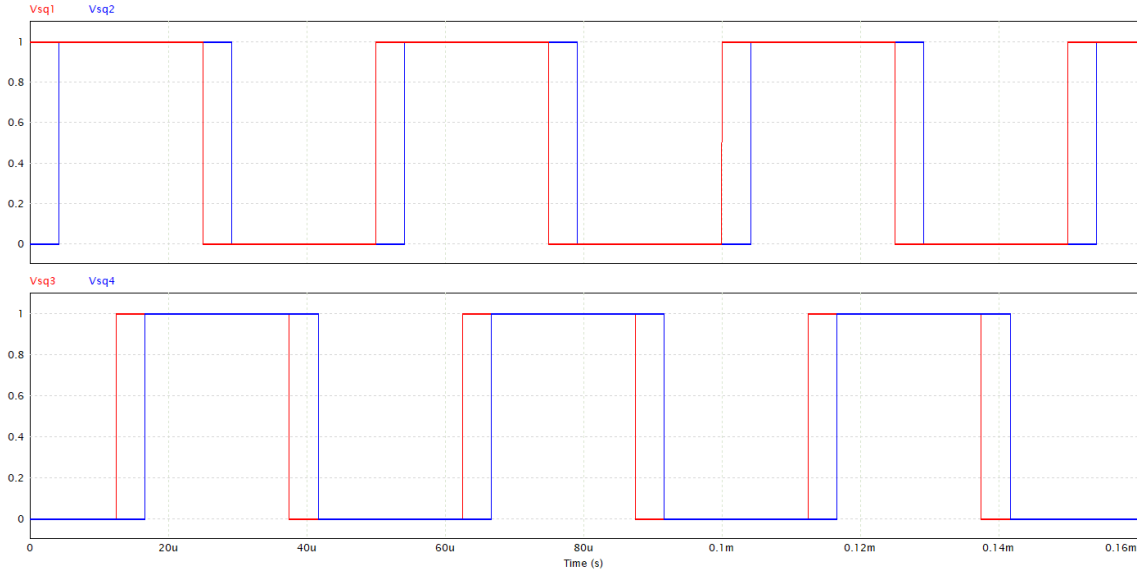

Figure 4.6: 30 degree phase shifted waves for first and second DAB.

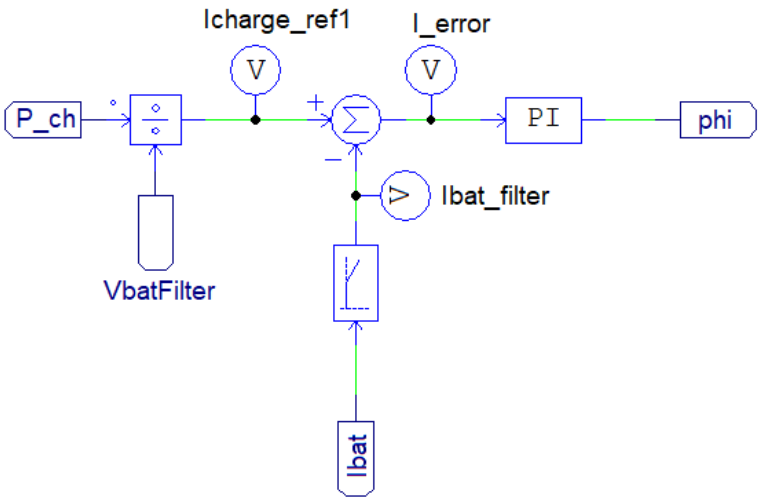

Figure 4.7: PI Controller Circuit on PSIM.

was that a power 100 kW was applied to the battery for the first seconds, constantly decreasing to 65 kW and maintaining it, the curve final seconds would vary depending on the test. Figure 4.8 and 4.9 shows a power charging curve example.

4.4 Results

4.4.1 30º vs 72º Phase Shift at Permanent Regime

Several simulations where carried out to observe the waveforms of the DAB in different conditions. The first run of simulations was to analyse the waveforms of the voltage in the primary and

```
Following variables are valid:  t, delt
                Input
                Output    y1

1  if (t < 2) {
2    y1 = 100000;
3  } else if (t < 2.8) {
4    y1 = -43750 * t + 187500;
5  } else if (t > 4) {
6    y1 = 0;
7  } else {
8    y1 = 65000;
9  }
```

Figure 4.8: C block code for power charging curve.

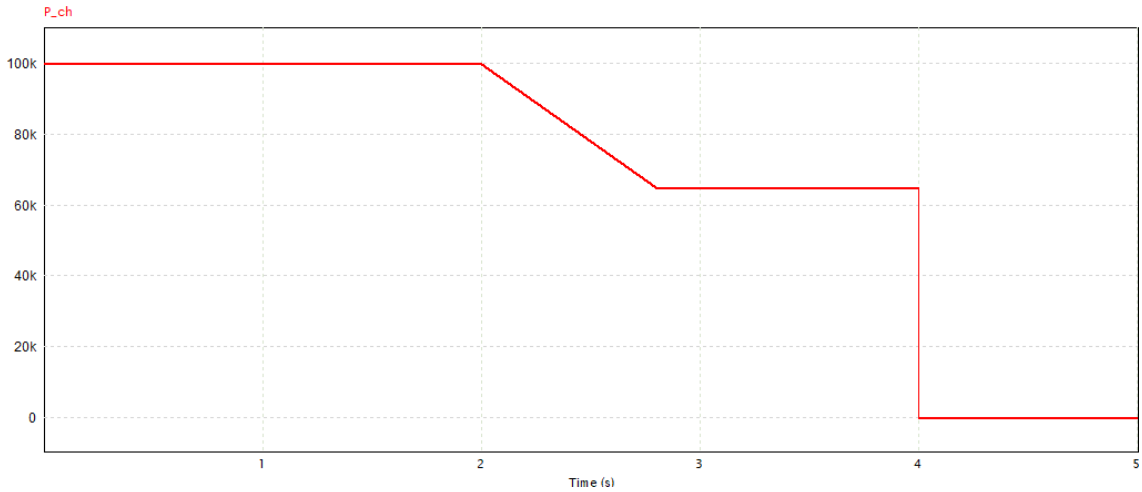

Figure 4.9: PSIM power charging curve graph.

secondary windings, as well as the voltage and current in the coil and its subsequent output current at different levels of phase shift.

Figure 4.10 and 4.11 show these waves with the converter performing at ϕ equalling 30º and 72º respectively. By analyzing the graphs disposed we can clearly see a larger shift implemented in the secondary square waves of figure 4.10a in comparison to figure 4.11a. This shift can also be seen in the voltage of the primary and secondary windings of the transformer. At the primary winding the square wave's peak voltage reaches 650 V, the V_i value, and after passing the 2:1 transformer it is reduced to 325 V in the second winding. These waves are shifted according to its introduced ϕ angle. Figure 4.10c and 4.11c, demonstrate the voltage and current in the coil. V_L reaches a maximum value of $V_i + V_o/n$ for the time that the primary wave leads the secondary (operating mode 1 of Table 3.1), and gets to $-(V_i + V_o/n)$ at operating mode 1' of Table 3.1. Operating modes 2 and 2' will give values of $V_i - V_o/n$ and $-V_i + V_o/n$, respectively. In the example these almost reach zero as the transformer ratio almost equals V_i to V_o/n. V_L and I_L show the AC component of the DAB.

Io demonstrates the DC rectification of the AC component of the DAB. As the angle ϕ increases, so does the the average of the current output. By comparing Figures 4.10d and 4.11d,

with 72 degree angle phase shift the current output maximum value increases, and so does it's average value. For ϕ=72º the power output reaches the maximum desired power of 100 kW while at ϕ=30º the power reaches around 58 kW.

4.4.2 Reverse Flow in Permanent Regime

To observe the bidirectionality of the DAB, the same waves on the previous subsection were analysed in permanent regime with an angle of ϕ=-30º. In Figure 4.12a and 4.12b the secondary wave leads the primary one, and as the theory suggests, this creates a flow towards the reverse direction. V_L and I_L follow the same principle as the previous explained waves. The main difference comes in the output current waves, at an angle ϕ of -30º the I_o wave is reversed in comparison to the original power flow. The average current in this graph obtains a negative value, which will thus give way to a reverse power flow in the converter.

4.4.3 PI Control Response

To inspect the transitory response of the converter, two reference power charging curves where coded, both had the same curve for the first 4 seconds, and after that the first reference in Figure 4.13a abruptly ends, while the second in Figure 4.13b constantly decreases until ϕ=-20º.

In these figures we can see in red the wanted power curve and in blue the power flow with PI response to follow the reference, in the graph below each figure there is the phi response that changes accordingly to obtain the power needed, with a maximum of 72º and a minimum in figure 4.13b of -8º.

The graphs in Figure 4.14 show an overview on output current against reference current. It is evident that the waveform of I_o decreases in size as the reference current decreases in value. This decrease in peak to peak value diminishes the average current flowing and thus the power adjusts to a lower level.

4.4.4 Step responses

The final simulations made had the objective to analyse the dynamic response of the output current's to a step in the reference current.

Figure 4.15a shows the response to a step to 0 A, through the figure after the suuden decrease in the reference current, the average current Io decreases rapidly, and reaching an average constant value of 0 A in 1.25ms. Figure 4.15b shows a step to a negative value, Io reaches a constant value in quicker fashion in 0.2ms.

4.4.5 Interleaved DAB

Further simulations were carried out, to also analyse the 2 level interleaved DAB, seen in Figure 4.2.

Figure 4.16a, shows the 20 kHz frequency square waves applied to the converter and, as seen in the theory development, the second PWM signal would be shifted 90º from the first. This same shift can be seen in the winding voltage (Figure 4.16b).

In Figure 4.16, several readings were made to the converter for analysis. In the first graph screen, the current at the output of the first bridge (Idc1) and second bridge (Idc2) as well as the current after the bridges (Ibat1) are shown. It is confirmed that the effective frequency at the output of the bridges are twice the switching frequency that the interleaved DAB operates, which propagates effective sharing of the load. Ibat2 and Vo1 show the values of current and voltage at the battery load simulator, this would equate these values to 115 kW.

4.5 Conclusions

With these simulations, the theory was put into practice by implementing the DAB converter in a real life DC charging station simulation. The converter was designed, attending to real life values, and the PI controller was developed and showed impressive responses, corroborating with the fluidness of the phase shift seen in Chapter 3, by following a charging curve with impressive reactions in regards to it's power output changes.

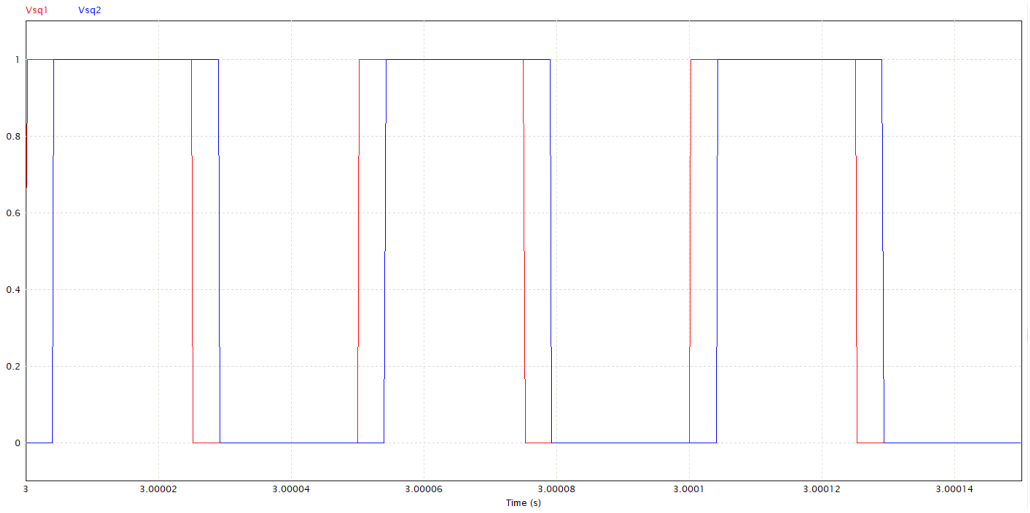

(a) Square waves with 30 degree phase shift.

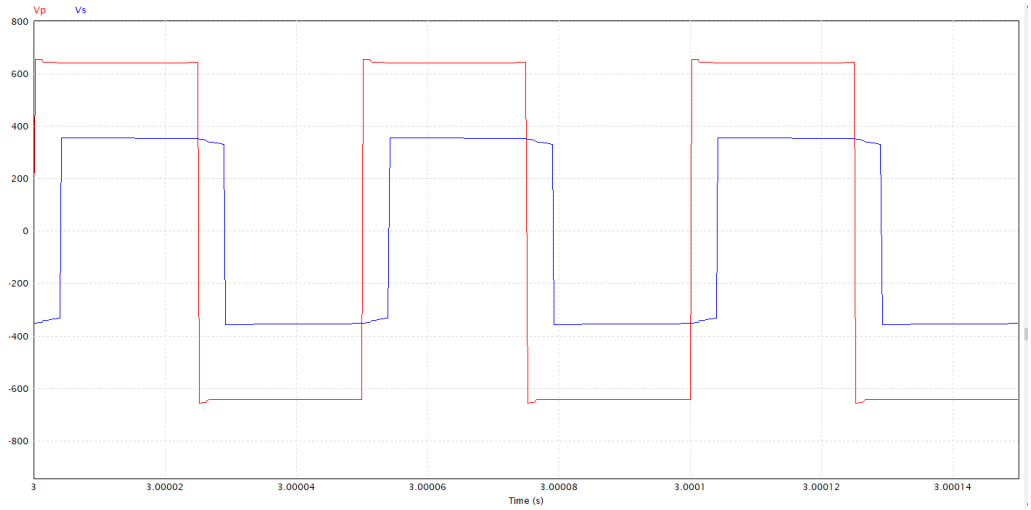

(b) Voltage in the primary and secondary windings of the transformer with 30 degree phase shift.

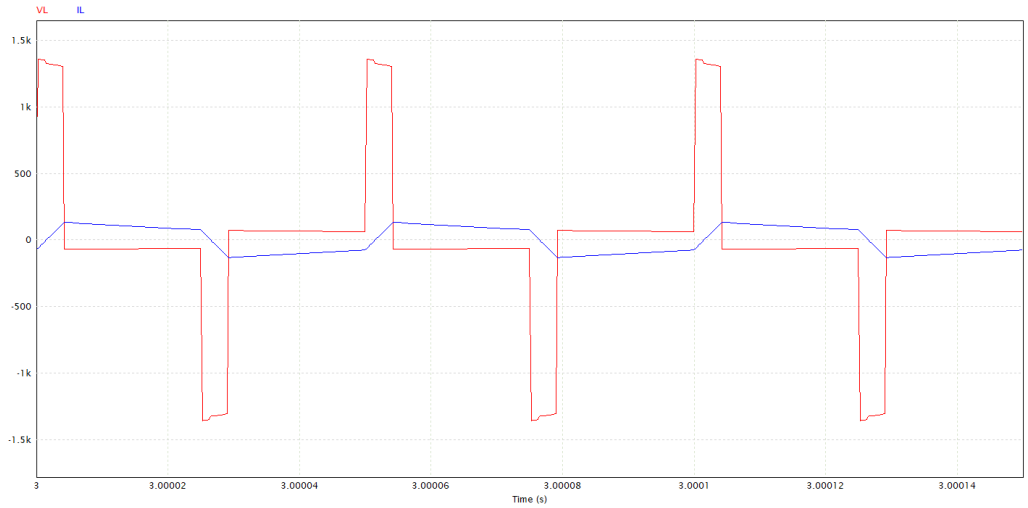

(c) Voltage and current on the coil with 30 degree phase shift.

Figure 4.10: Waveforms for 30 degree phase shift.

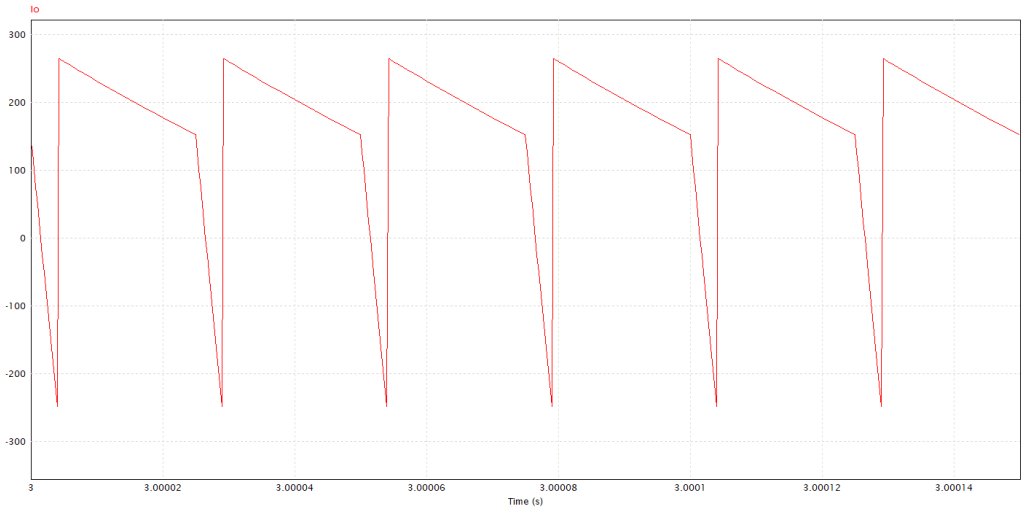

(d) Current output with 30 degree phase shift

Figure 4.10: Waveforms for 30 degree phase shift.

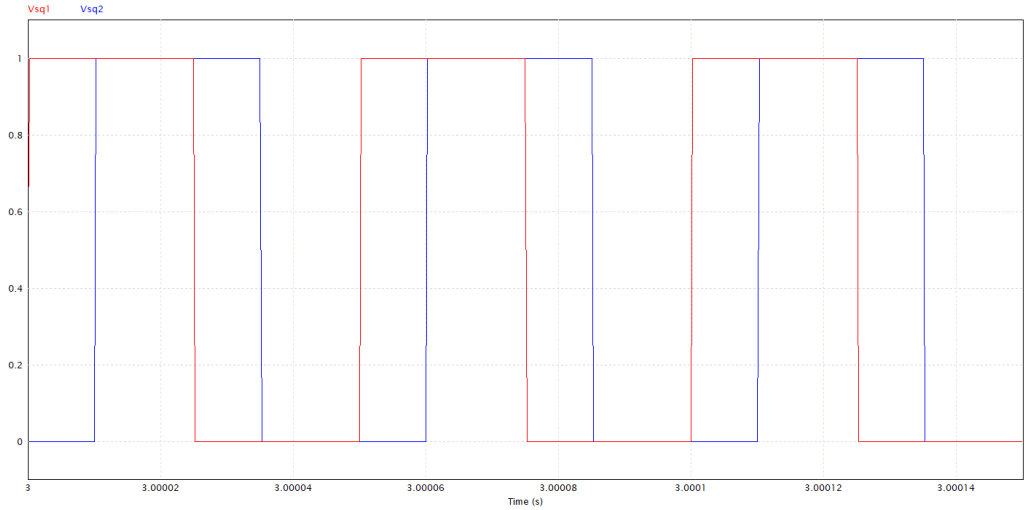

(a) Square waves with 72 degree phase shift.

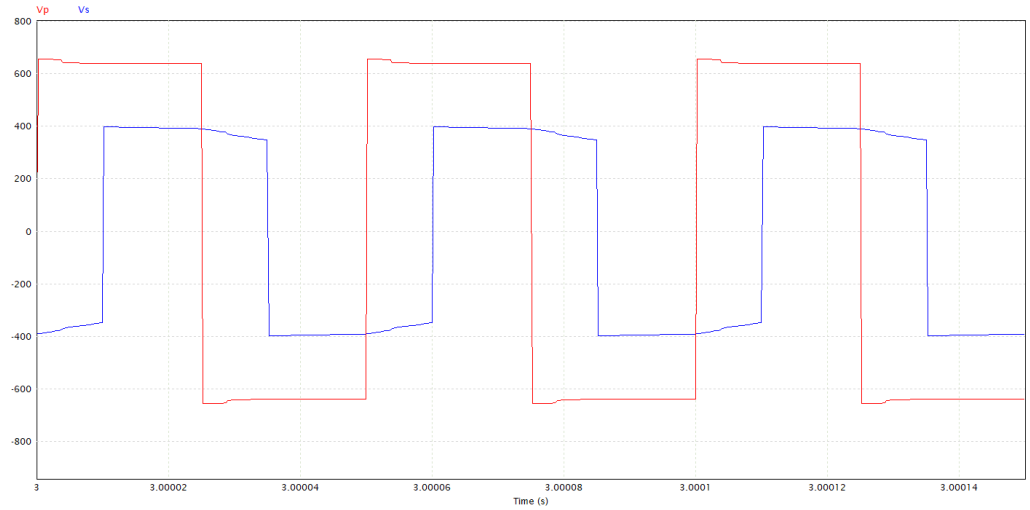

(b) Voltage in the primary and secondary windings of transformer with 72 degree phase shift

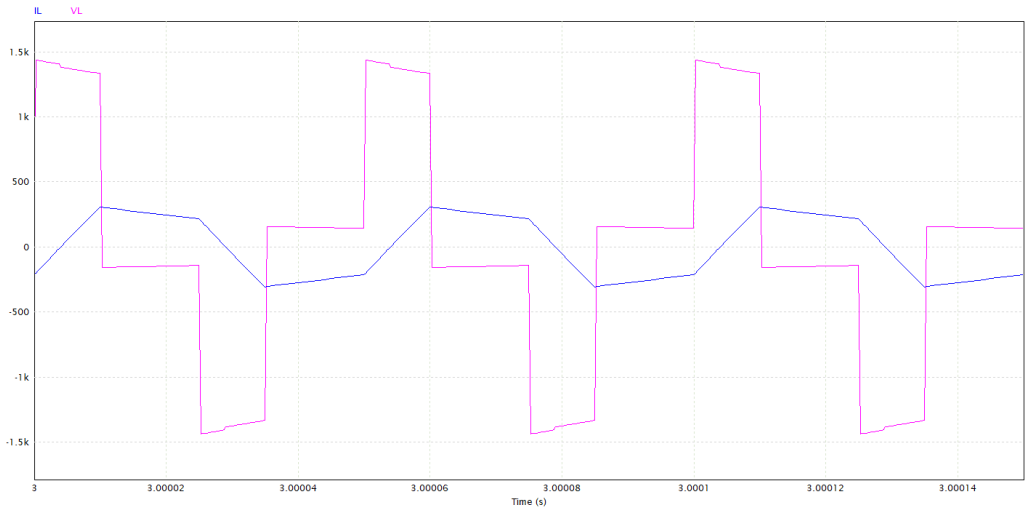

(c) Voltage and current on the coil with 72 degree phase shift

Figure 4.11: Waveforms for 72 degree phase shift

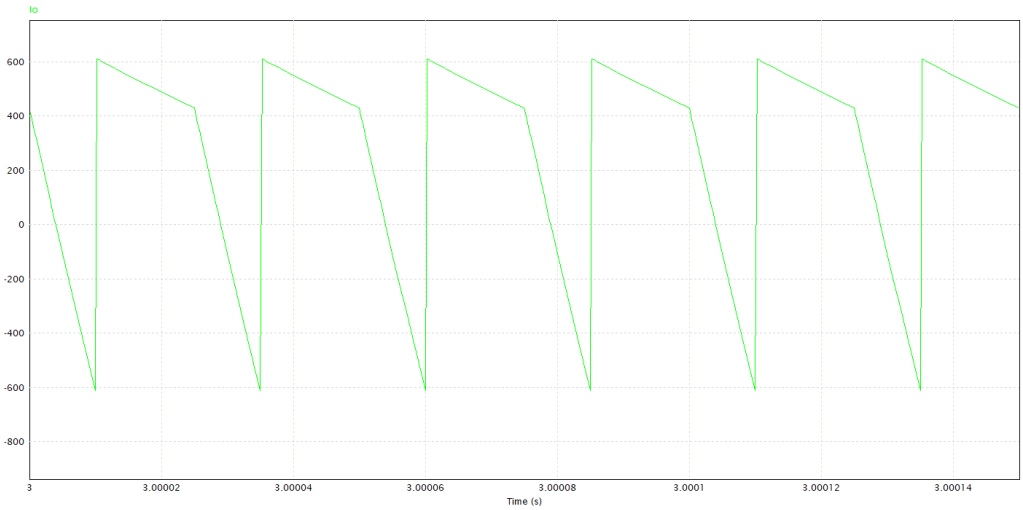

(d) Current output with 72 degree phase shift

Figure 4.11: Waveforms for 72 degree phase shift

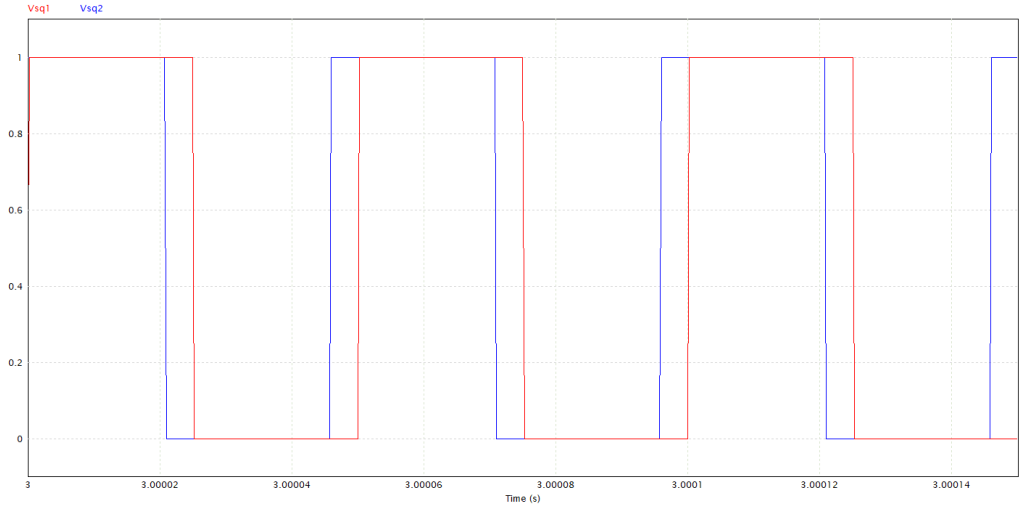

(a) Control signals: square waves with a negative 30 degree phase shift

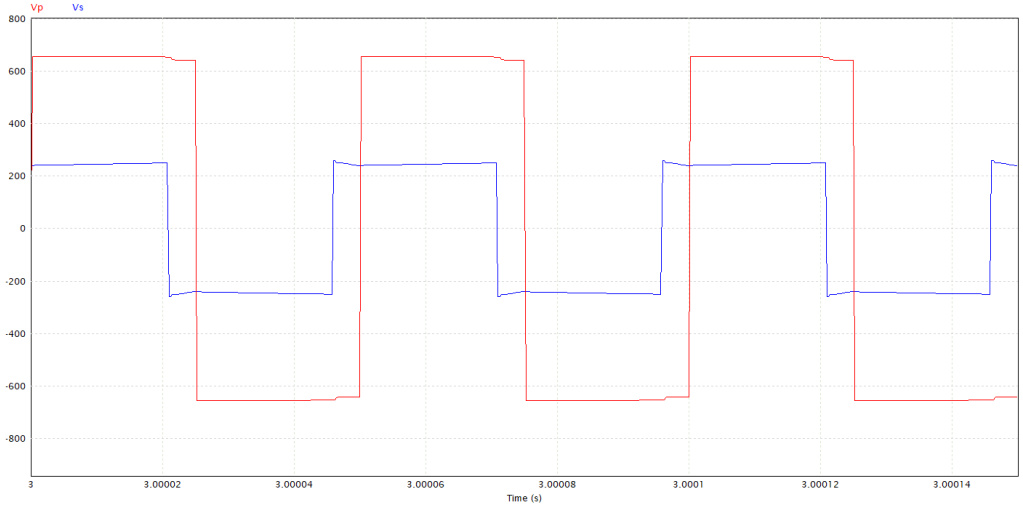

(b) Voltage in the primary and secondary windings of transformer with a negative 30 degree phase shift

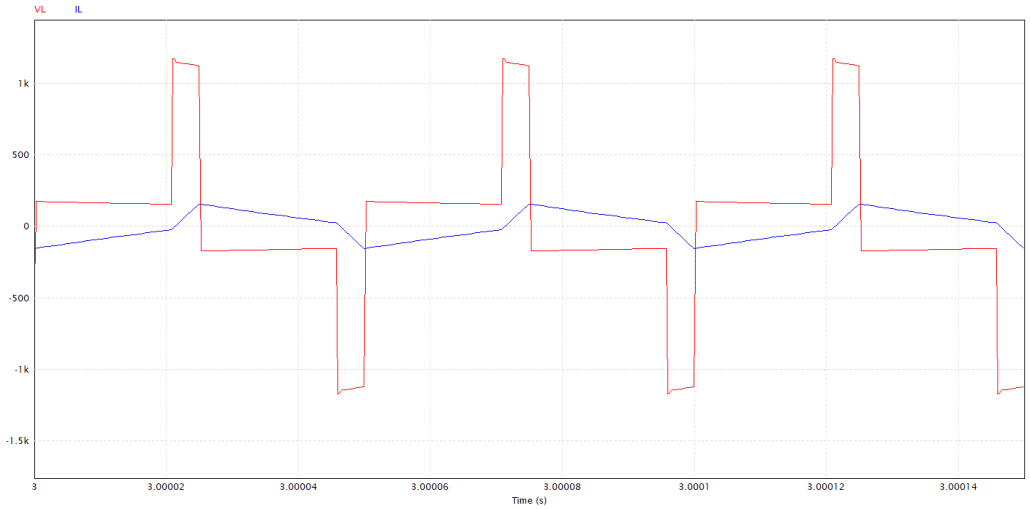

(c) Voltage and current on the coil with a negative 30 degree phase shift

Figure 4.12: Waveforms for a negative 30 degree phase shift.

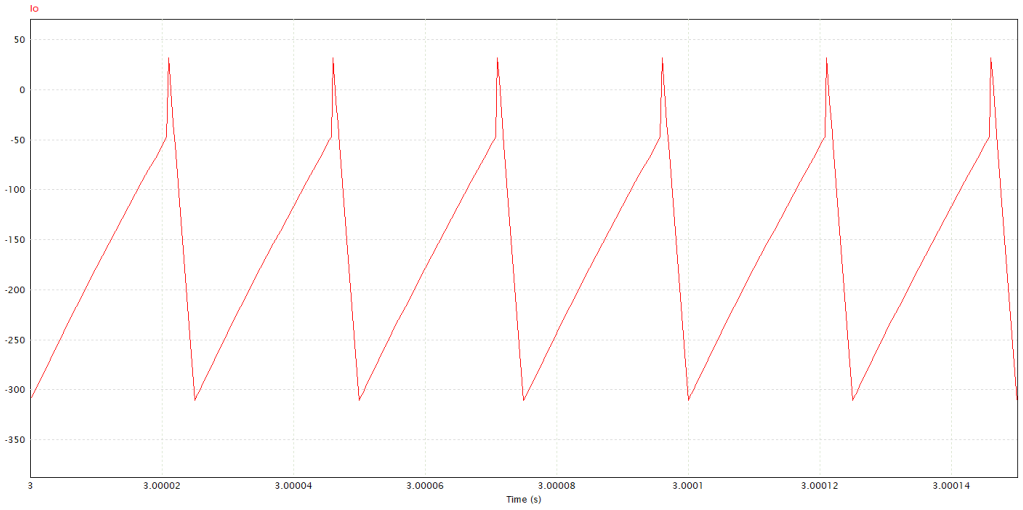

(d) Current output with a negative 30 degree phase shift

Figure 4.12: Waveforms for a negative 30 degree phase shift.

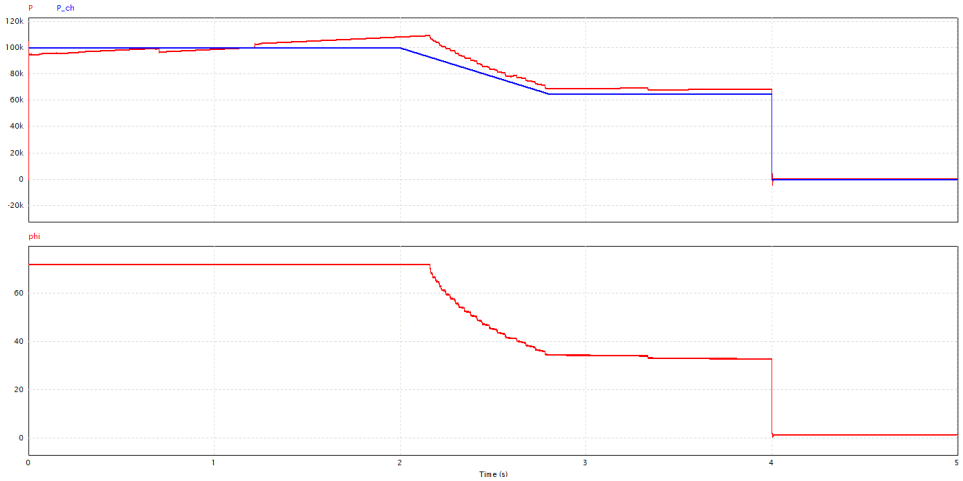

(a) Charging power and angle phi response with abrupt end.

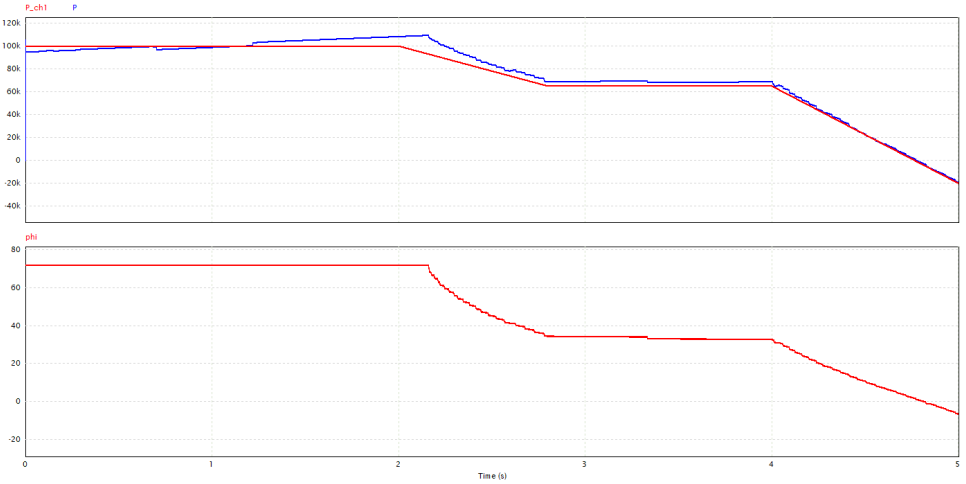

(b) Charging power and angle phi response with power flow switch

Figure 4.13: Waveforms for the charging power and angle phi PI response.

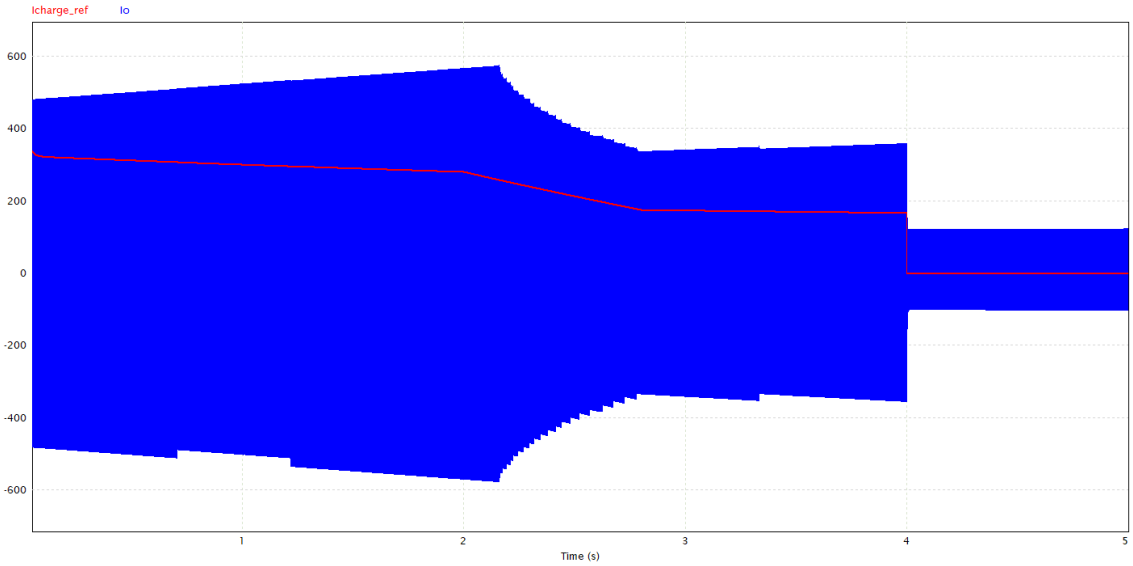

(a) Overview of output current with reference power to 0 kW

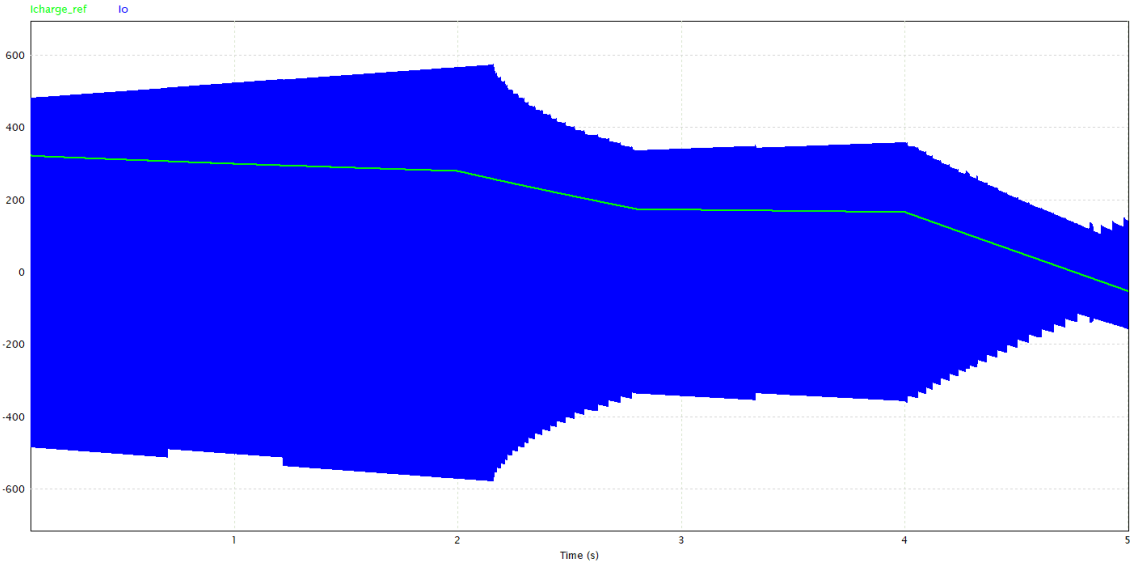

(b) Overview of output current with reference power to -20 kW

Figure 4.14: Overview of output current against reference current.

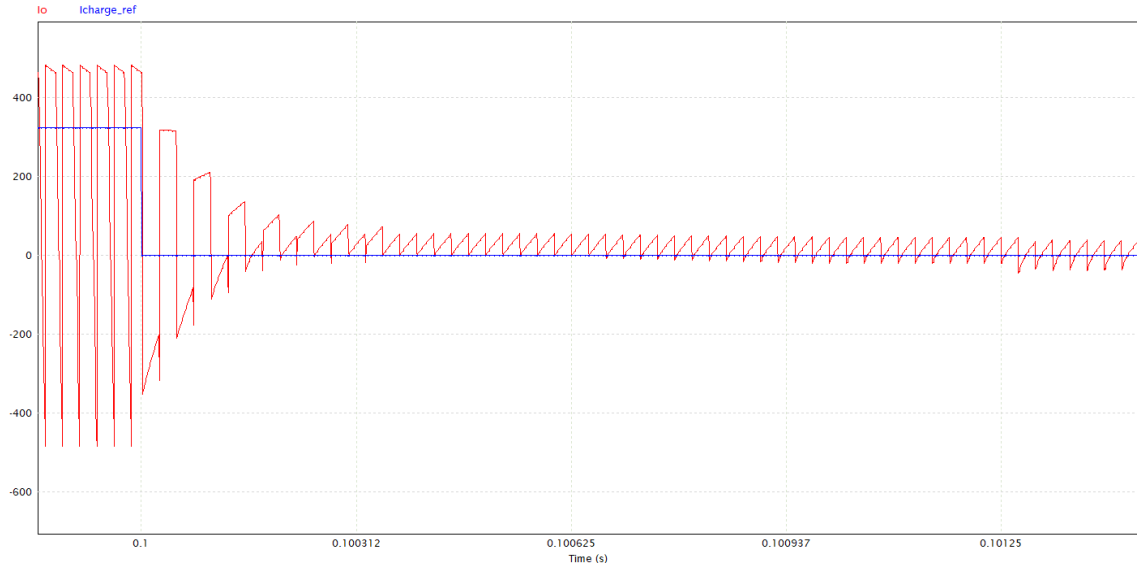

(a) Zoomed output current step response to 0 kW

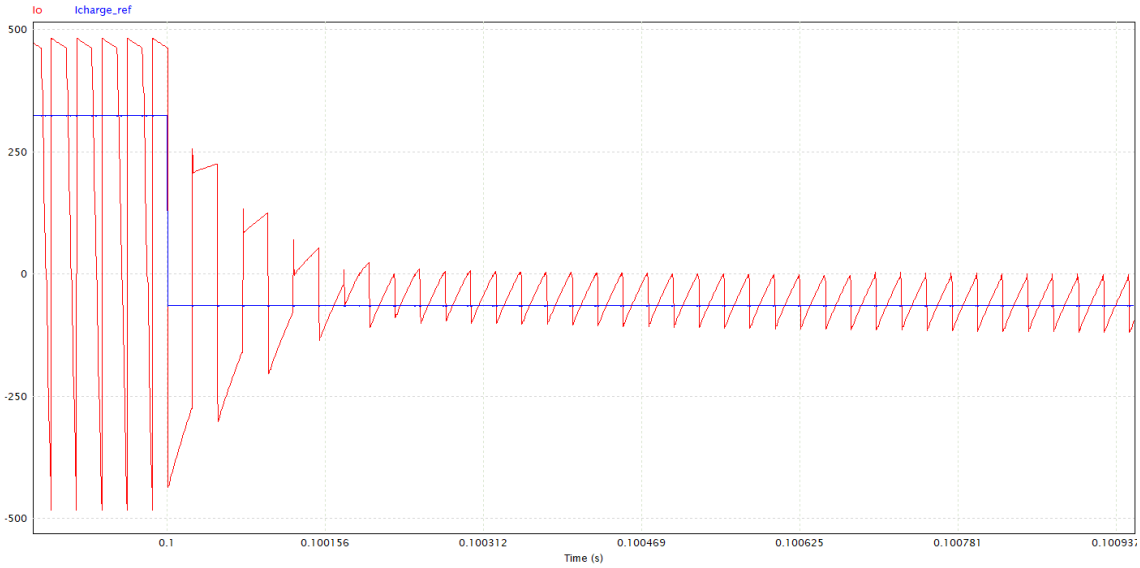

(b) Zoomed output current step response to -20 kW

Figure 4.15: Zoomed waveforms for the output current step response.

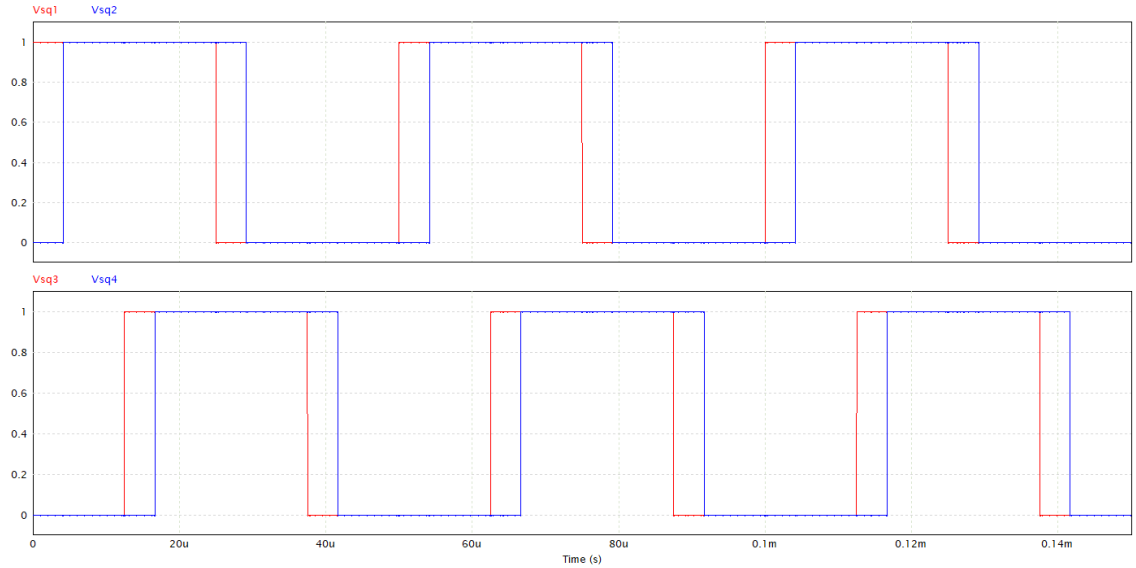

(a) Square waves with a 30 degree phase shift

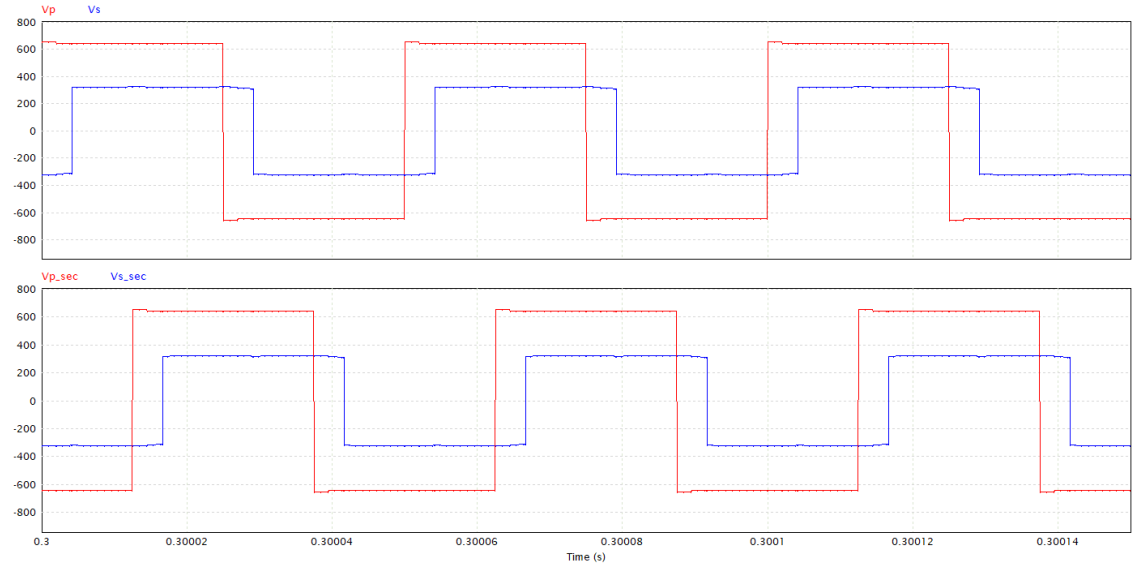

(b) Voltage in the primary and secondary windings of both transformers with a 30 degree phase shift

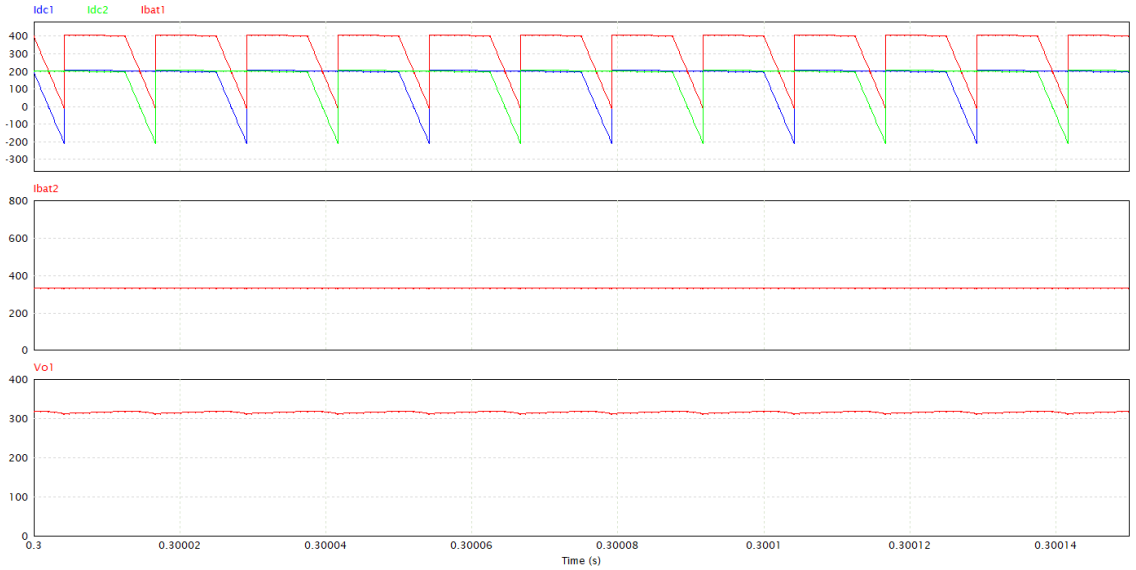

(c) Voltage and current on the coil with a negative 30 degree phase shift

Figure 4.16: Waveforms for interleaved DAB with 30 degree shift.

Chapter 5

Experimental Test

After the simulation process, experimental work was started to test the DAB in scaled real conditions, with hardware. For this tests to work out the microcontroller must be chosen and the square waves implemented, as well as the values of voltage input picked, as well as the transformer and coil calculated.

It was established that the DAB would work at a frequency of 20 kHz and would receive a DC input of up to 60 V, a value sacaled by 10 compared to the PSIM simulation.

5.1 Microcontroller

The choice of microcontroller, that would be used to control the waves, fell to the STM32F429 [5.1]. It is a microcontroller from the STM32F4 series, which is a family of based on the ARM Cortex-M4F architecture. The STM32F429 is typically used in applications that require high performance and a wide range of connectivity options, such as in medical devices, industrial control systems, and consumer electronics. This controller might be over the top for the DAB control proposed. However, due to having slight contact with it in past classes, interest was gained in evolving the knowledge in this realm. This model is based on a nucleus of 32bits and can work at frequencies of up to 216 MHz. It offers 13 timers and its pins at "HIGH" value are limited to 3.6 V.

5.1.1 Square Wave Implementation

To control the DAB, as the theory suggests, 4 waves must be implemented, 2 of them complementary to one another and with phase shift, when compared to the first. For this, the following configurations must be made:

1. Clock configuration;
2. Timer configuration;
3. Dead Time insertion;

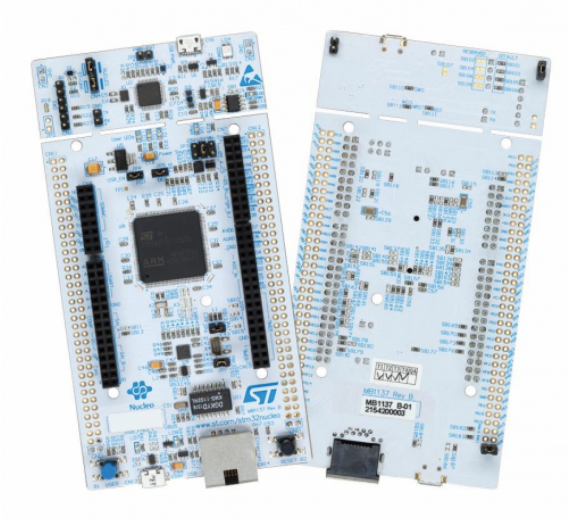

Figure 5.1: STM32F429 Development Board.

4. Signal declaration on the firmware.

5.1.1.1 Clock Configuration

On the clock configuration interface, in the STM32CubeIDE software, a value of 25MHz was set for the system clock.

5.1.1.2 Timer Configuration

For the timer configuration, the idea was to set up 3 timers, each with 1 set of complementary waves. These timers would be triggered by the previous timer, to allow for the phase shift between complementary pairs. Figure 5.2, shows the timer interface.

To obtain the PWM waves, the "PWM Generation channel" was chosen at each timer, and for this wave to work at 20 kHz calculations were made using the following equations:

$$TIM.CLOCK = \frac{APB.TIM.CLOCK}{PRESCALAR} \tag{5.1}$$

$$frequency = \frac{TIM.CLOCK}{ARR} \tag{5.2}$$

$$DutyCycle(\%) = \frac{CCR}{ARR}100 \tag{5.3}$$

APB.TIM.CLOCK is the system clock that was set to 25 MHz, and by knowing the desired frequency of 20 kHz, the calculation lead to the values that can be seen on Figure 5.2: PRESCALER set to 5 and AutoReloadRegister (ARR) set to 250. The values were subtracted by 1 as in the STM32 the starting bit is 0.

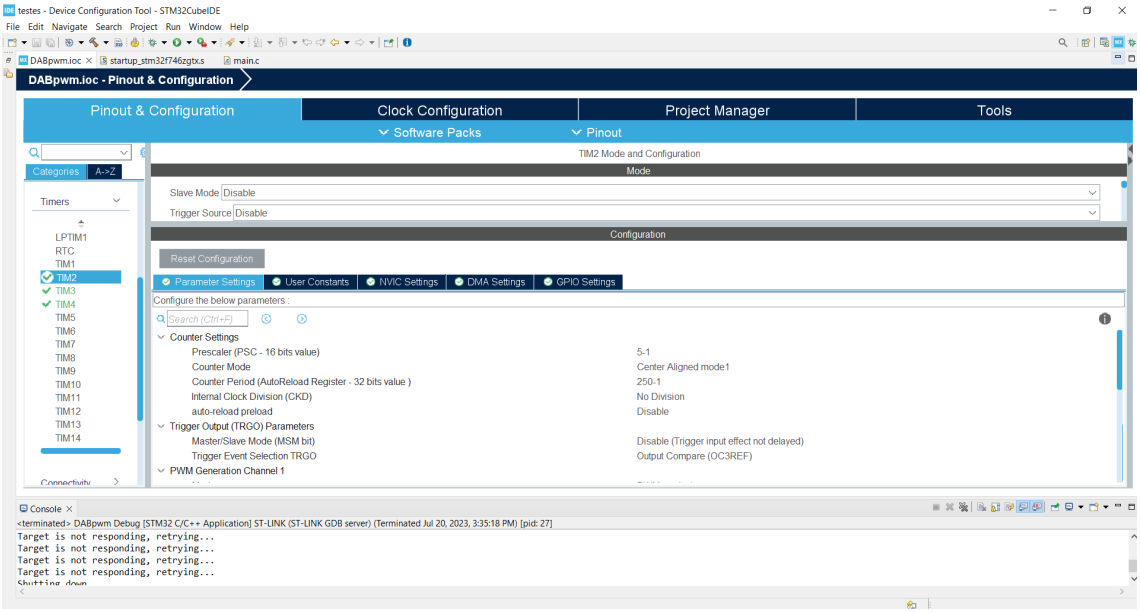

Figure 5.2: STMCubeIDE timer interface.

After setting up the frequency of the wave, the PWM wave must be set up. For this project the PWM was generated in centre align mode. Figure 5.3 shows the main function of the center align mode, it allows for the PWM to be built in the center permitting easier control of the phase shift if bidirectional flow is applied. A comparison between the center aligned and usually standard edge aligned mode can be observed in Fig.5.4.

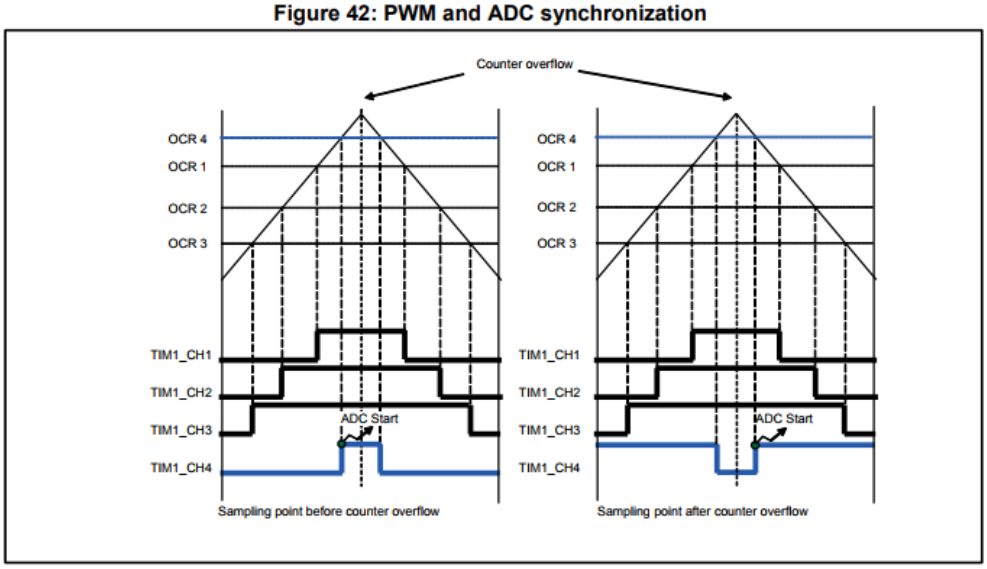

Figure 5.3: Centre align mode principle, [8].

The trigger control is an essential component for the phase shift to work was the configuration

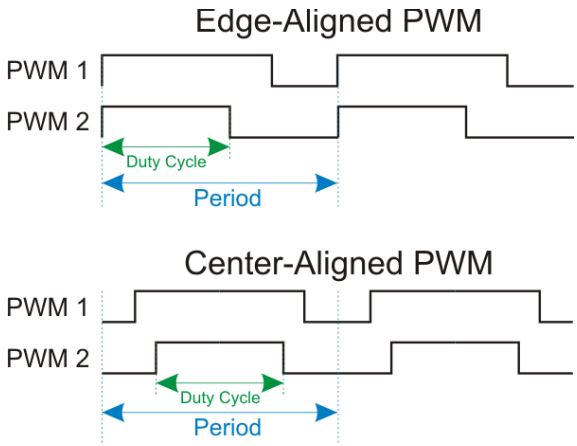

Figure 5.4: Centre align mode comparison to edge aligned, [9].

of the triggers and for each timer to work as a master or slave. Table 5.1 shows the internal trigger connections between timers.

Table 5.1: Internal Trigger Connections

Slave TIM	**ITR0**	**ITR1**	**ITR2**	**ITR3**
TIM2	TIM1	TIM8	TIM3	TIM4
TIM3	TIM1	TIM2	TIM5	TIM4
TIM4	TIM1	TIM2	TIM3	TIM8
TIM5	TIM2	TIM3	TIM4	TIM8

For the project in hand, the three timers initialized were: TIM2, TIM3 and TIM4. TIM 2 would act as the PWM in the primary bridge, TIM 4 would act as the PWM for the secondary bridge, and TIM3 acts as a trigger intermediary to apply the phase shift between TIM2 and TIM4. For this, both TIM3 and TIM4 work in slave mode activated by the signal ITR1 and ITR2 respectively, meaning TIM3 is a slave of TIM2 and TIM4 a slave of TIM3. To control the angle ϕ, an ouput compare channel (OCC) was inserted in the master timers (TIM2 and TIM3), these channels would activate the PWM signal of their respective slaves when they changed from LOW to HIGH and the timing of this switch could be controlled by the pulse of the OCC, thus controlling the phase shift.

Figure 5.5 has an example of the implemented timers and output compares. Timer 2 has two PWM generators complementing each other and an output compare that sets to one after the pulse value time has passed, counting from the beginning of the timer initialization. This switch will activate it's slave, which in this case is TIMER 3 and the same will happen to the slave/master dynamic between TIMER3 and TIMER4.

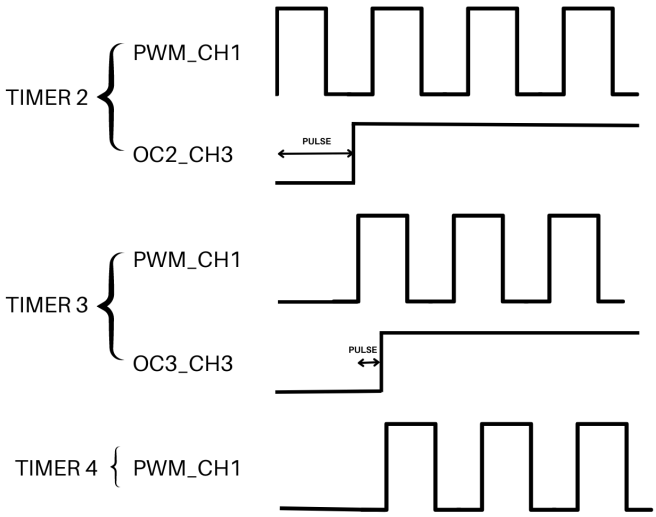

Figure 5.5: Output Compare with active level on match.

5.1.1.3 Dead Time Insertion

An extremely important factor for the safe behavior of the converter is the insertion of dead time in the PWM square waves applied to the transistors. This will allow for the soft switching of the ZVS bridges of the DAB. The dead time is the time that must exist between the commutations in a leg, and must be high enough so that that the ON/OFF switching does not occur simultaneously.

For the waves at a 20 kHz frequency, a full period will take 50 us, for this time period a dead time of 1us was chosen which equates to about 2% of the full period. It was implemented by altering the duty cycle of the complementary waves, and as they were in centre align mode, by having the duty cycle HIGH proportionally lower to when its LOW, an adjustable dead time was created.

5.1.1.4 Signal Declaration on the Firmware

After the timer initialization, it is necessary to declare the signals. For this objective, the HAL library was used in the STMCubeIDE.

Figure 5.6 shows the code that initializes the timers and GPIOs, then it writes the value of the phase shift by chasing the prescale value of the OC on channel 3 of TIMER3. After that it declares all the PWM's and OC's generated.

5.2 Transistor Control

The transistor control system is isolated by optocouplers, which are used to protect control circuits, normally with low voltage/current, from more dangerous circuits involving high voltages and currents. For the correct operation of these optocouplers, it was necessary for the signal to

```
MX_GPIO_Init();
MX_TIM2_Init();
MX_TIM3_Init();
MX_TIM4_Init();

TIM3->CCR3=50;

HAL_TIM_PWM_Start_IT(&htim2, TIM_CHANNEL_1);
HAL_TIM_PWM_Start_IT(&htim2, TIM_CHANNEL_2);
HAL_TIM_OC_Start_IT(&htim2, TIM_CHANNEL_3);
HAL_TIM_PWM_Start_IT(&htim3, TIM_CHANNEL_1);
HAL_TIM_PWM_Start_IT(&htim3, TIM_CHANNEL_2);
HAL_TIM_OC_Start_IT(&htim3, TIM_CHANNEL_3);
HAL_TIM_PWM_Start_IT(&htim4, TIM_CHANNEL_1);
HAL_TIM_PWM_Start_IT(&htim4, TIM_CHANNEL_2);
```

Figure 5.6: HAL library code for signal declaration

transmit 5V with a minimum current of 10 mA. The microcontroller STM32F429 signals were of voltage and current lower than necessary, and so, a buffer, the CD4050 was used [34]. This buffer allows the placing of several input signals to the same level voltage, which will be the buffer's supply voltage, in this case the PWM signals will go from 3.6 V to 5 V. To increase their current, each of these signals was connected to 3 buffers in parallel.

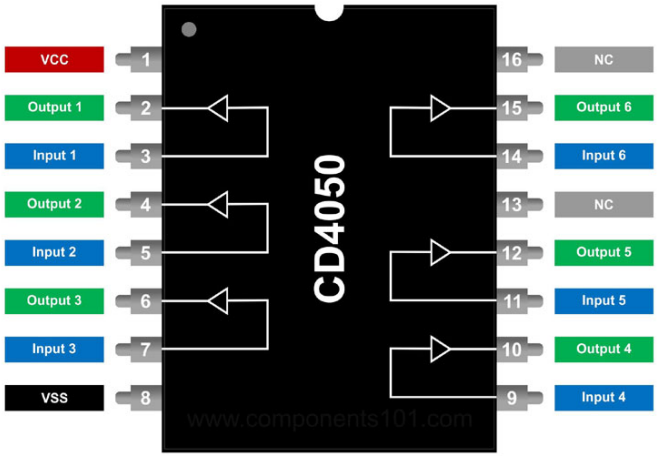

Figure 5.7: CD4050B CMOS Hex Inverting Buffer

5.3 Circuit Build and Setup

For the DAB circuit build the hardware utilized included:

- DC Voltage Source;
- 2x 1ph inverter driver (H-bridge) (Figure 5.8);
- Medium frequency transformer;

- Coil;
- DC electronic load.

The DC Voltage source used for the input voltage of the converter would be able to reach up to 60 V and would connect to the first 1ph inverter driver with a SK25GH063 module [35]. The second 1ph inverter driver was connected to the first after the coil and transformer series circuit. The DC electronic load used was the BK Precision 8500 that could receive a maximum input power of 300 W [36].

A 100 uH coil was welded in series with the transformer, as shown in Figure 5.9. This transformer was built with a turns ratio of 40:22, which, at a maximum primary voltage of 60 V the secondary voltage would decrease to around 33 V, a ratio of 1:0.55. The ferrite used was EE42, which was an appropriate option for the power and frequency of the experimental project [37] [38].

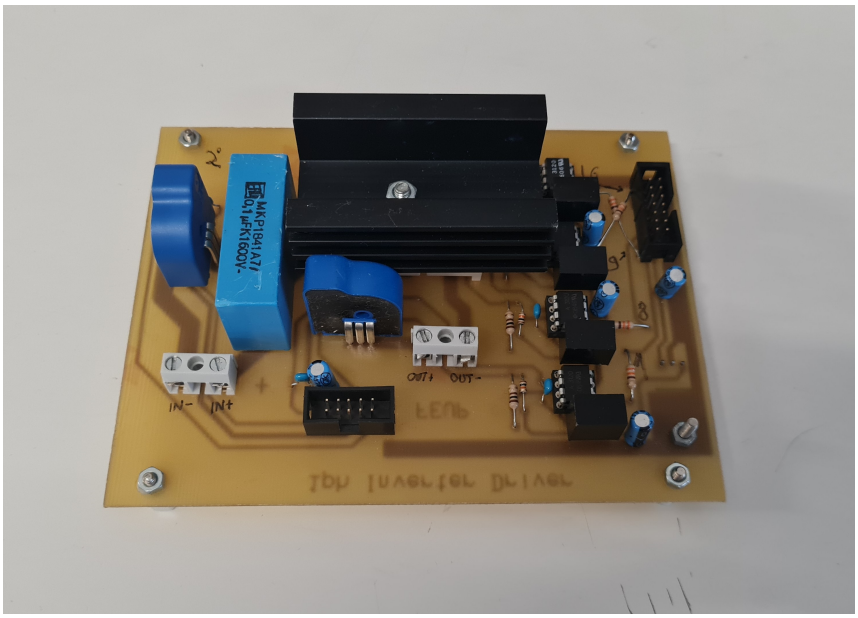

Figure 5.8: Single phase inverter with current sensors.

To control the switching of the experimental prototype and input the PWM signals defined by the microcontroller and enhanced by parallel buffers, a 14 pin connector makes the coupling between the signals and the 1ph inverter. Figure 5.10a shows the circuit layout of the 1ph inverter and Figure 5.10b shows the layout of the 14 pin connector.

After pre-testing all the hardware and joining them as explained earlier, the full ecosystem for the DAB to work was finished and ready for testing. Figure 5.11 shows the full DAB converter circuit built, with isolated voltage and current probes and test equipment.

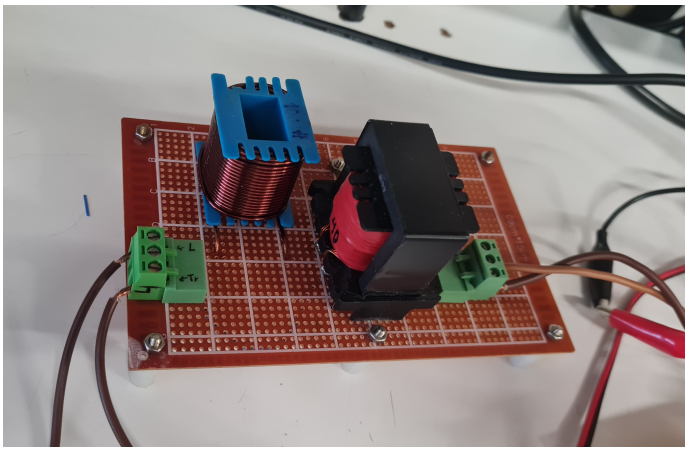

Figure 5.9: Coil and transformer series circuit.

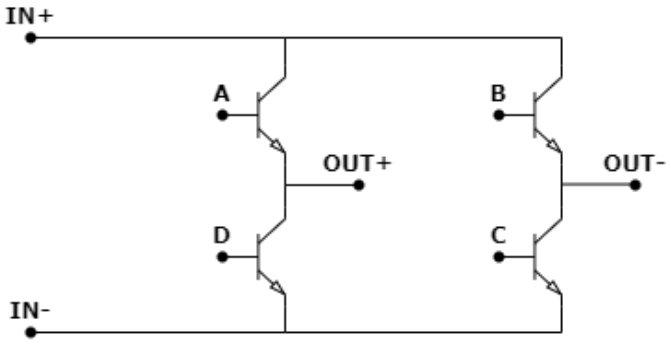

(a) Single phase inverter, SK25GH063 module layout

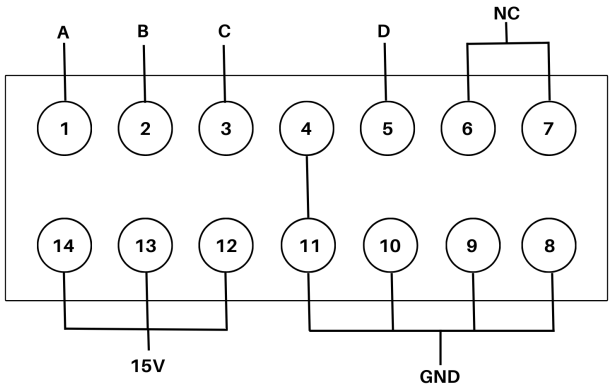

(b) Connector pinouts

Figure 5.10: Connector pins and bridge circuit diagram.

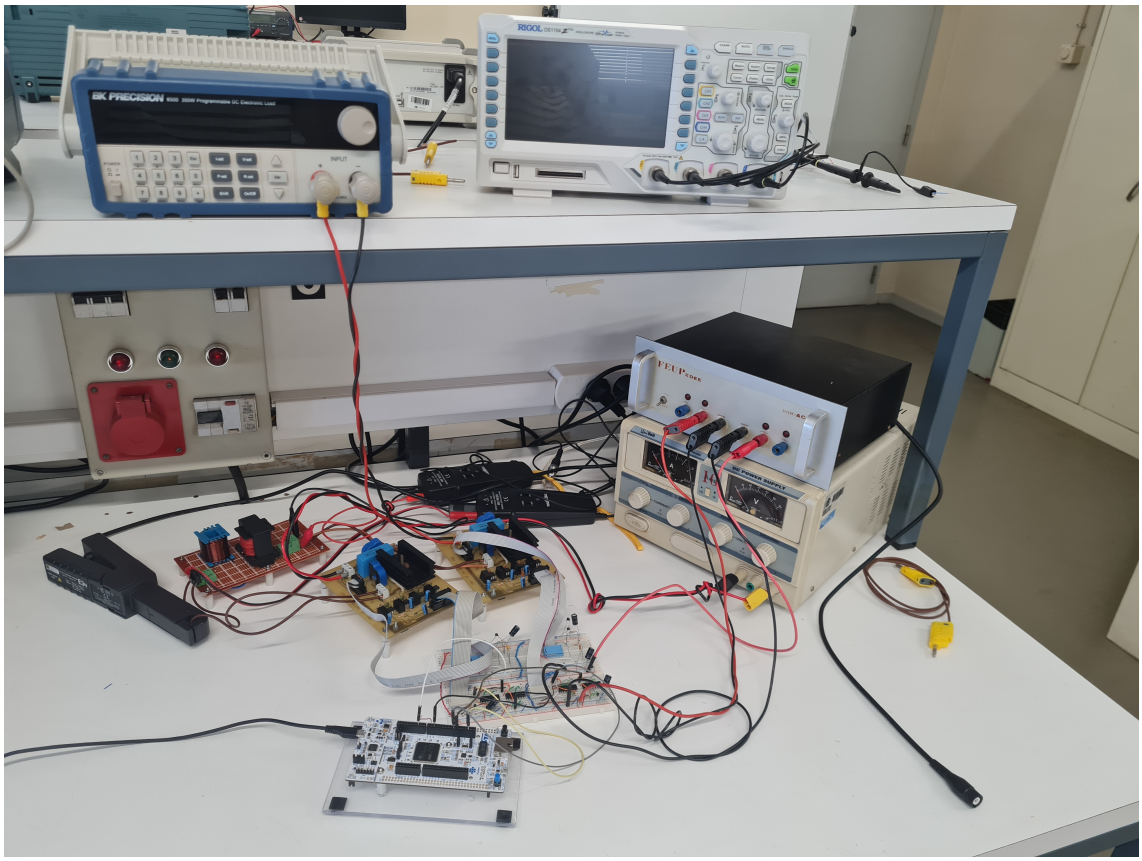

Figure 5.11: Full DAB circuit build.

5.4 Results

5.4.1 Preliminary Testing

Before the functional test at maximum power, preliminary testing is needed to guarantee the correct operation of the hardware. The first requirement is the right PWM signal with sufficient dead time produced by the microcontroller as described previously. Figures 5.12 shows the different conditions surpassed in the PWM signal implementation. 5.12a shows the complementary signal that is applied to the first bridge with a 1us dead time, which is confirmed in Figure 5.12b, with the zoomed signal at 1us per square in the oscilloscope.

Figure 5.12c shows the attainable, variable phase shift between the PWM waves, in this case with an angle ϕ of 30º. For the bidirectional characteristic the following Figure 5.12d, shows the phase shift with ϕ at -30º.

To test the bridge modules, previous testing was also made by applying the PWM signals to only one of the bridge while the other would act as a diode bridge. Both bridges were confirmed to be operating without problems and figure 5.13 shows the results on the oscilloscope of this final preliminary test.

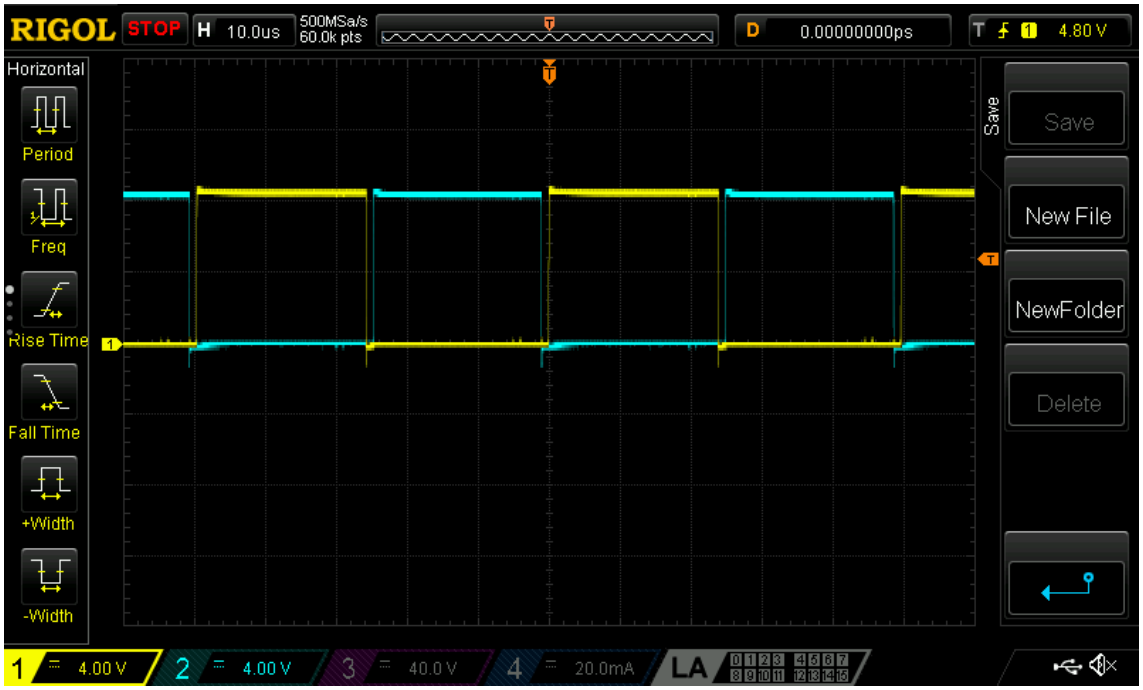

(a) Complementary PWM waves with dead time

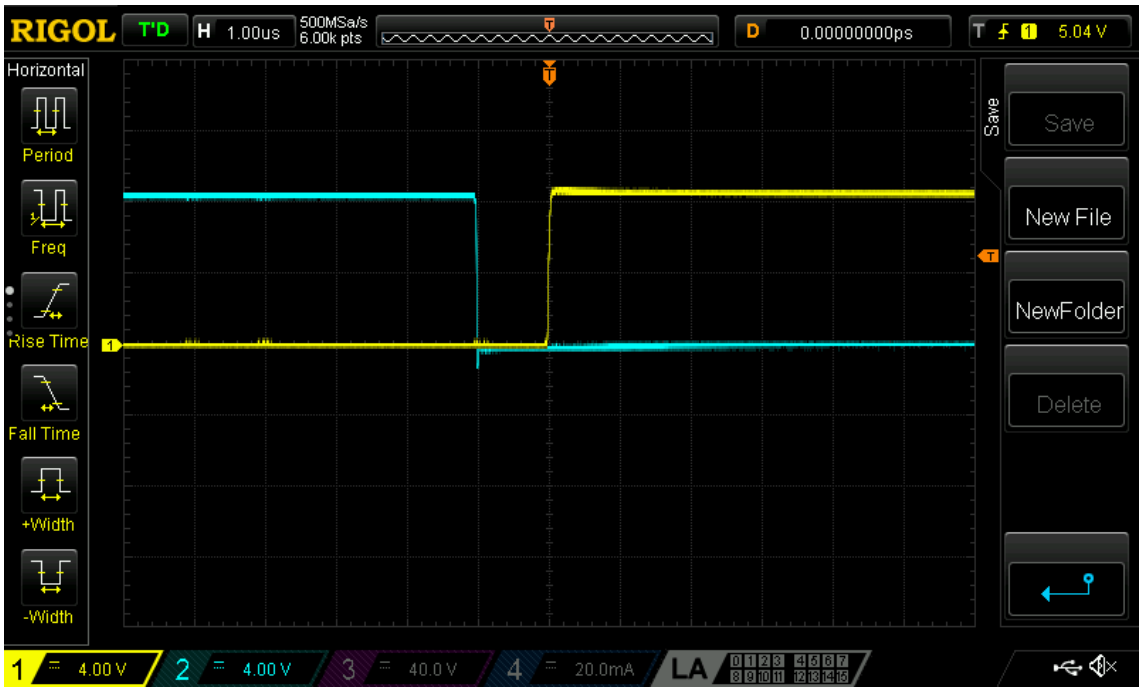

(b) 1us dead time

Figure 5.12: PWM signal confirmation.

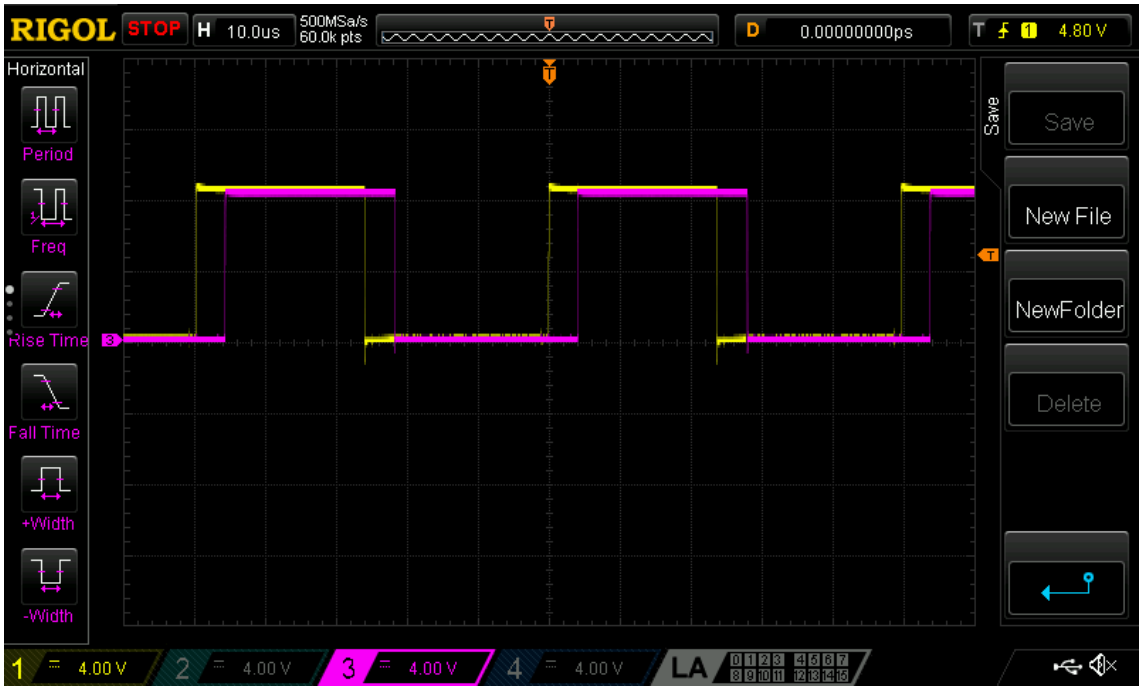

(c) PWM at ϕ=30º

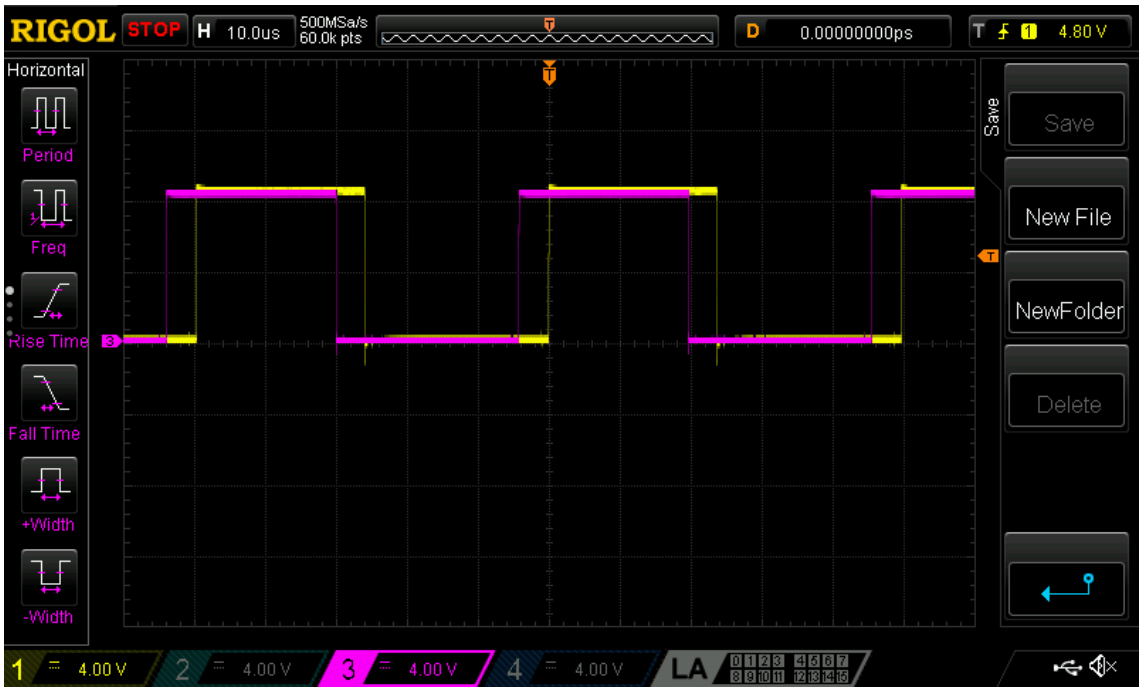

(d) PWM at ϕ=-30º

Figure 5.12: PWM signal confirmation.

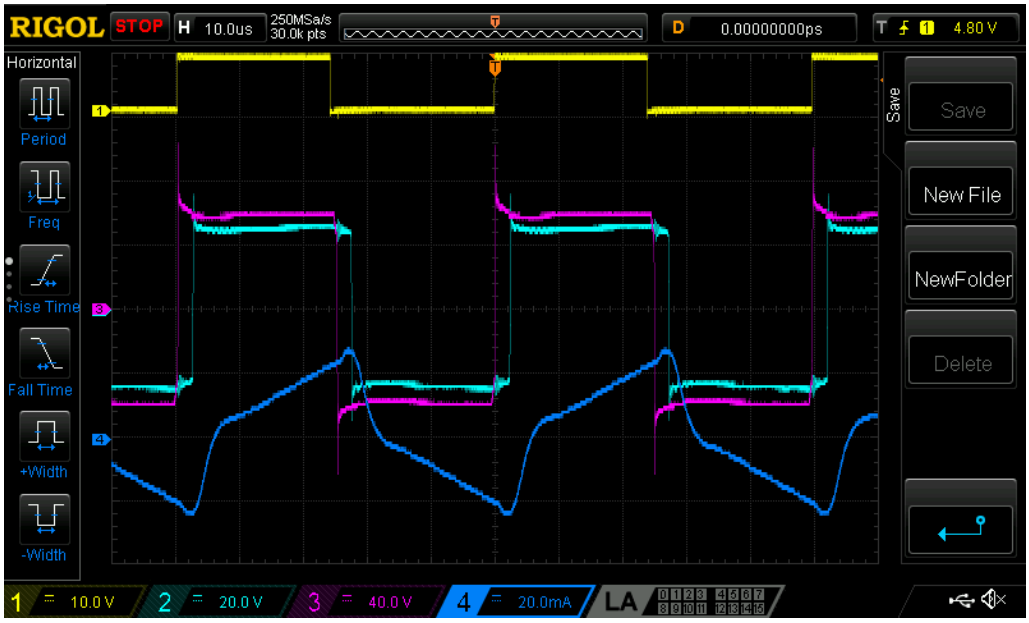

Figure 5.13: Full bridge and diode bridge test result. Yellow: PWM; magenta and light blue: primary and secondary voltages; dark blue: primary AC current.

5.4.2 DAB testing

After corroborating the hardware components and signals, the DAB could be finally tested, to analyse the waveforms of the primary and secondary windings, as well as the current I_L at angle phase shift of ϕ = 30º, 0º and 60º.

The first analysis was to observe the waves at an angle of 30º, with the maximum set voltage value of the load of 24 V. Figures 5.14, shows the electric load values (5.14a) and the oscilloscope waves (5.14b). The waves presented show in yellow and light blue, the voltage in the primary winding (V_p in figure 3.1), before the coil, and the voltage in the secondary winding (V_s in figure 3.1), respectively. These measurements shows the difference of 30º in angle between both bridges, and their peak value represent the input Voltage (60 V) in the primary winding and output voltage in the secondary (24 V). In pink, the I_L shows the AC component, the electric load receives 3 A, which will equate to an output power of 72 W.

When increasing the electric load voltage from 24 V to 36 V, the respective waves (Figure 5.15b) change in comparison to Figure 5.14b. The peak voltage in the secondary winding will increase, turning I_L from boost to buck, as n = 0.55 and with the new value of load voltage, 36 V/0.55 = 65 V, slightly higher that 60 V. This environment will operate with an output power of 94.3 W.

The second test would alter the angle ϕ to 60 degrees and revert the electric load voltage back to 24 V. The V_p and V_s relation (Figure 5.16b) would thus be similar to Figure 5.14b, however with larger phase shift, which will increase the power output as it was observed in Chapter 2. Current I_L has a bigger area when comparing to the previous examples, the AC component will lead to a bigger average current to the output, and as seen in Figure 5.16a, the highest current value was recorded, 4.43 A which will equate to 106.32 W.

The final test would be at ϕ=0, as could be noted by the overlapping V_p and V_s waves in 5.17b. The current going to the load equals 0.58 A, not a null value and the I_L still has a small AC wave. This is due to the reactive power still flowing and possibly the PWM signal phase shift may not exactly be equal to 0 (it should be noted that the tests were made in open loop).

5.5 Conclusions

This chapter presented the experimental phase of the dissertation, where further knowledge on the practical applications of the DAB where observed. During this process, a thorough implementation of the PWM signal waves was made with the use of the microcontroller STM32F429, with careful considerations on the voltage levels applied to the transistors and crucially on the dead time insertion to allow ZVS. In this portion of the dissertation more problems were faced in comparison to the PSIM simulation due to its nature of testing and confirming the right behaviour of the components to check for any flaws.

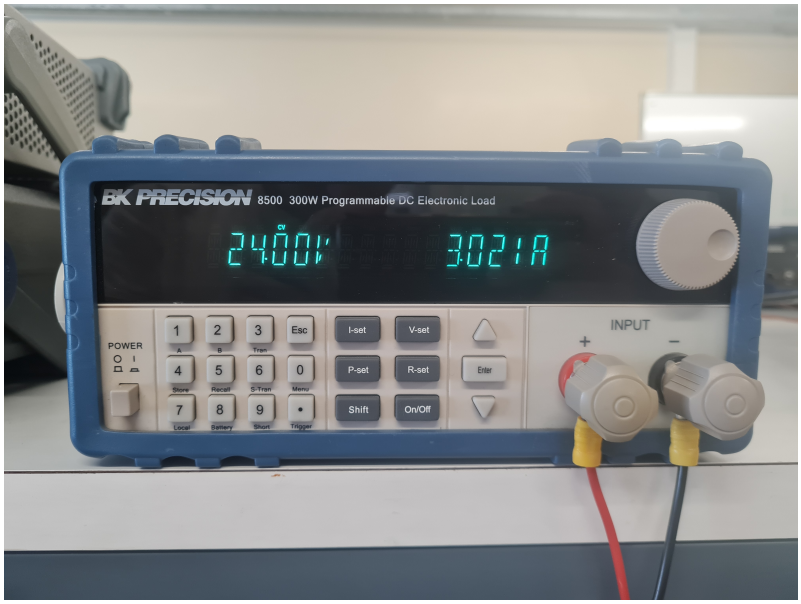

(a) Electric load values (Voltage and current input) with maximum 24 V set.

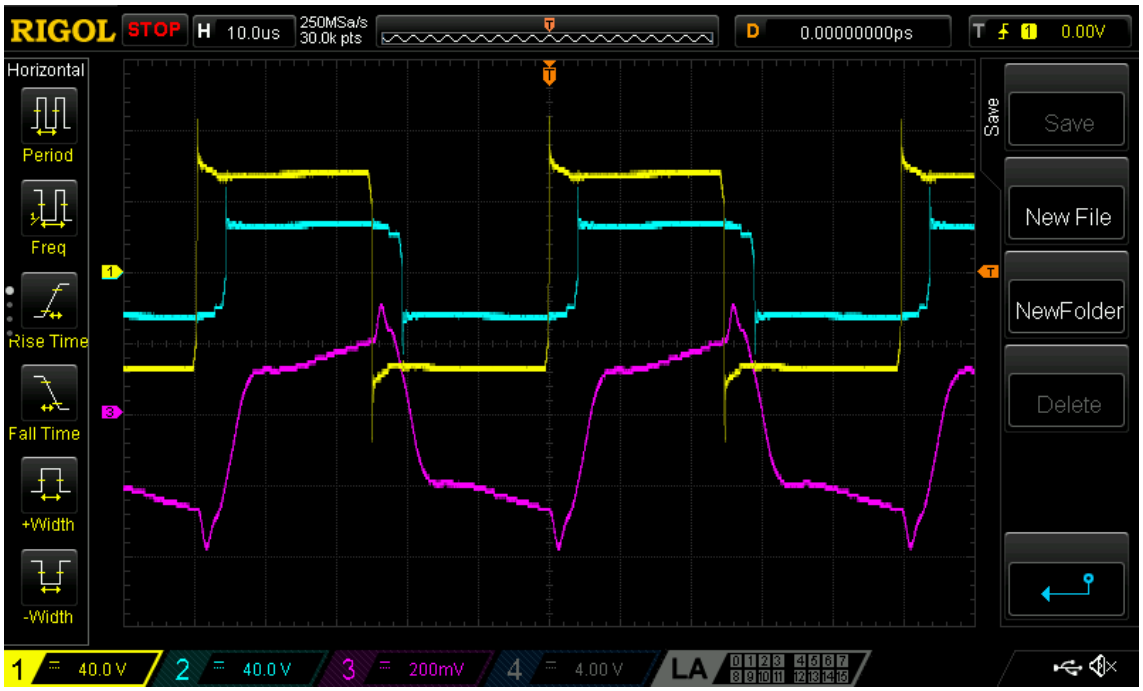

(b) Oscilloscope waves

Figure 5.14: Testing results for DAB at 30º angle phase shift and load voltage of 24 V.

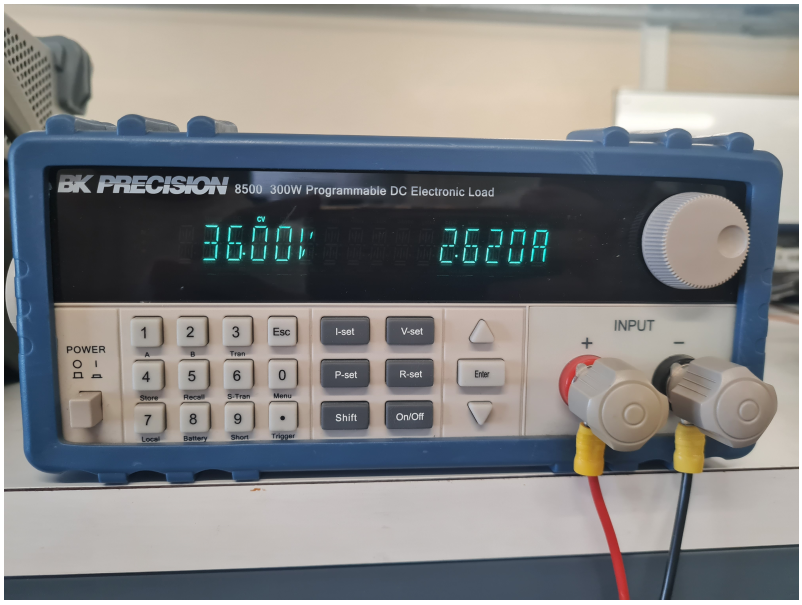

(a) Electric load values (Voltage and current input) with maximum 36 V set.

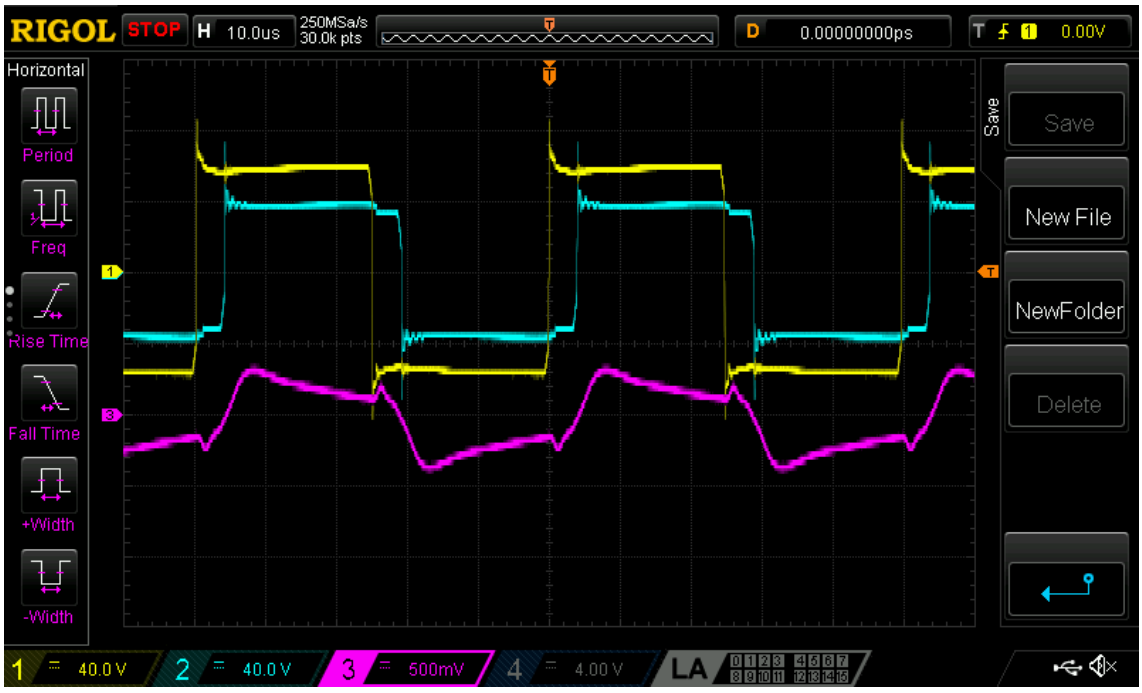

(b) Oscilloscope waves

Figure 5.15: Testing results for DAB at 30º angle phase shift and load voltage of 36 V.

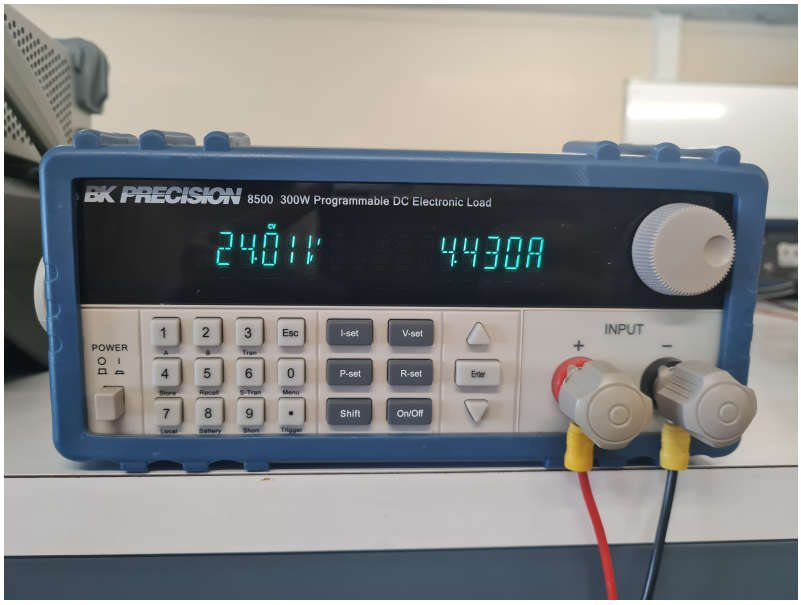

(a) Electric load values (Voltage and current input) with maximum 24 V set.

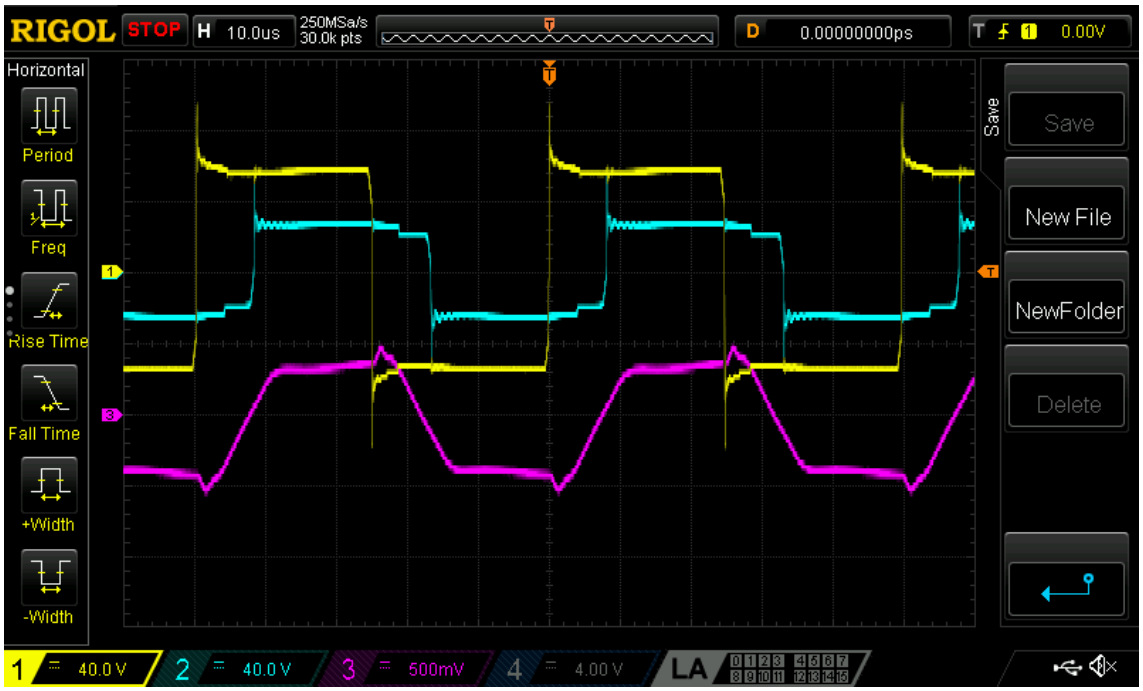

(b) Oscilloscope waves

Figure 5.16: Testing results for DAB at 60º angle phase shift and load voltage of 24 V.

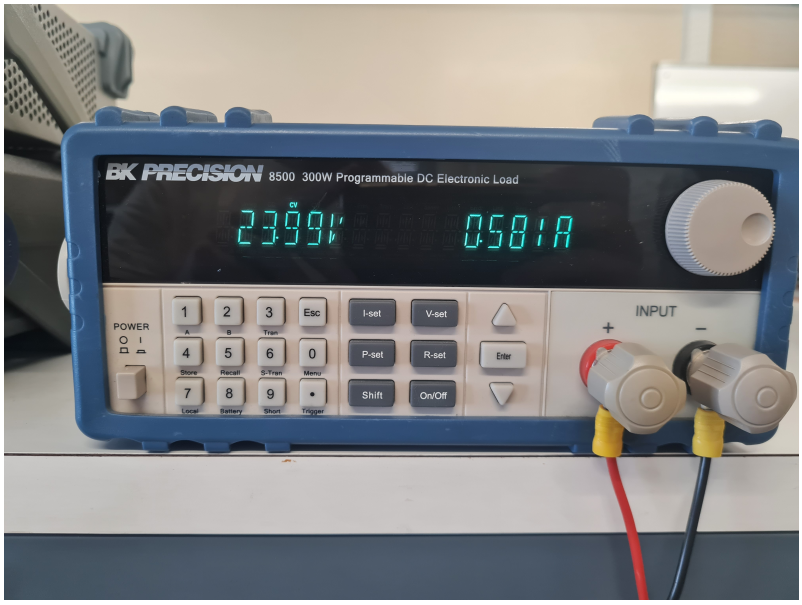

(a) Electric load values (Voltage and current input) with maximum 24 V set.

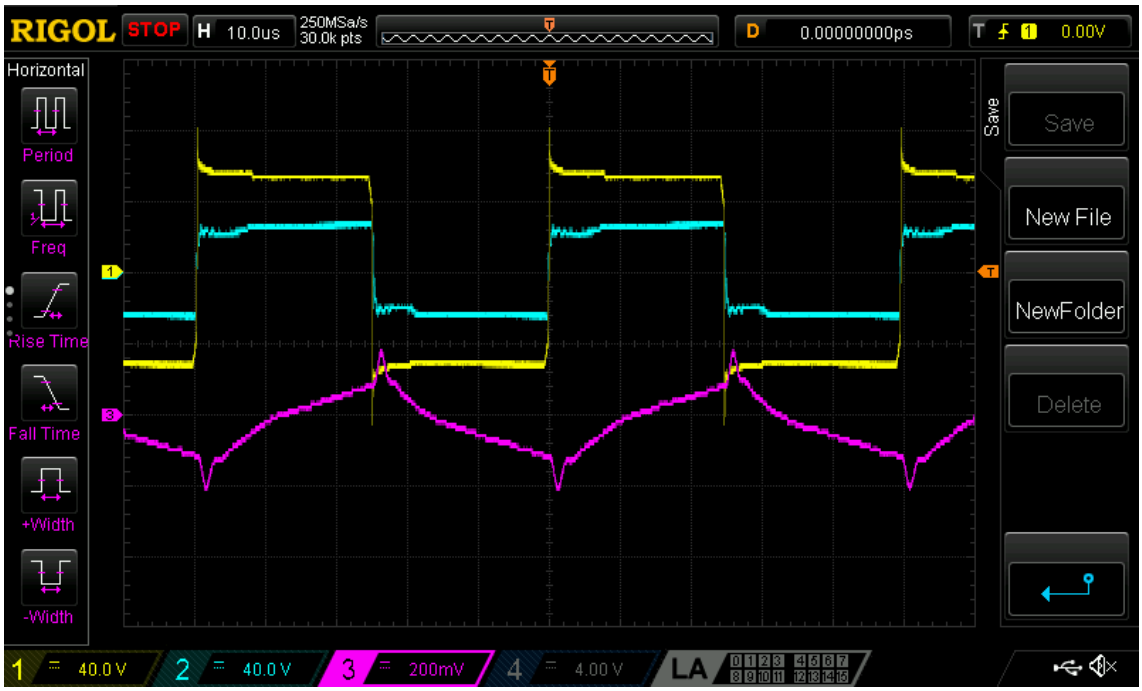

(b) Oscilloscope waves

Figure 5.17: Testing results for DAB at 0º angle phase shift and load voltage of 24 V.

Chapter 6

Conclusions and Future Work

6.1 Conclusions

As seen throughout this document, it is evident that the electric mobility market is increasing substantially and with this growth, EV charging stations must be up to par with the growing demand. The DAB converter will certainly be essential to this growth due to the many advantages explained in this thesis. This study delved into the theory of this power converter and its contextualization in regards to EV charging.

Several PSIM simulations were made where the performance of the DAB was evaluated in different conditions. The essential waveforms for its proper operation was examined and further analysis in terms of varying phase shift, not only with static evaluations, but also the dynamic alterations with its control tactic implemented was made to observe the impact on the power output given to the vehicle's battery. Among with these tests, its important bidirectional capabilities, modular construction and the interleaved DAB were closely checked, to verify its V2G capabilities and to understand the many complexities and the versatility of the converter at hand.

Furthermore, practical experiments of the DAB were put into place to observe and evaluate the converter without the ideal conditions of a virtual simulation, simulating a scaled environment where the DAB converter would operate inside a DC EV charger. From the choice of the components and to the decision on the testing values, these experiments were executed with careful step by step testing on the individual components to guarantee safe conditions for the desired results. Through the experiment the essential DAB waveforms were obtained and the impact that the phase shift inserted by the microcontroller on the H-bridges had on a load was examined, corroborating on the theory presented in previous chapters.

In conclusion, the DAB was extremely impressive due to its power range and fluid power flow. Its efficiency can be optimized with a more robust controller design and with minimization of switching losses, and with its optimized abilities it is a perfect suite for a DC fast charging station, either from its fluid power output control to protect the car battery or because of it's simple integration with V2G operations that may arise in the future.

Power electronics are crucial for EV evolution and this converter may in the future be one of the main proponents of electric mobility throughout the world.

6.2 Future Work

After the completion of the work detailed in the document, additional testing conditions were tried for a more complete understanding of the DAB in real conditions. More specifically a transient analysis of the converter. In this trial, the phase shift would change to evaluate in the oscilloscope the instant change in current value when ϕ change from 0 to 30 degrees. However, due to the microcontroller's output compare reset time, the PWM wave's frequency inserted to the converter would change at the instant of the angle shift, thus compromising the integrity of the converter and validity of the results obtained.

With more time to gain experience with the microcontroller chosen, or by altering the choice made, there would be several future testing that could be made to enrich this work, all relying on altering conditions in a continuous test. The instant of direct change of angle would be an interesting experiment to run, and further down the line a full control strategy, which in this case would be the PI control, could be tested to analyse its efficiency and real life performance. With a real battery used as the load, testing the bidirectional V2G component would be an incredible test to run for a complete, full DAB for EV charging at scaled condition testing.

References

[1] International Energy Agency. World Energy Data, 2022. URL: https://www.worldenergydata.org/world-electricity-generation/.

[2] H. Ritchie, M. Roser, and P. Rosado. CO2 and Greenhouse Gas Emissions. *Our World in Data*, 2020. URL: https://ourworldindata.org/co2-and-greenhouse-gas-emissions.

[3] go-e GmbH. Ac-dc charging. https://go-e.com/en/magazine/ac-dc-charging.

[4] EV Database. Volkswagen ID.4 Pro. https://ev-database.org/car/1627/Volkswagen-ID4-Pro.

[5] S. A. Gorji, H. G. Sahebi, M. Ektesabi, and A. B. Rad. Topologies and control schemes of bidirectional DC–DC power converters: An overview. *IEEE Access*, 7:123994–124017, August 2019. doi:10.1109/ACCESS.2019.2937239.

[6] J. Nan. A comparative study of three-phase dual active bridge and single-phase single-stage converters for EV charging applications. *Arizona State University*, 2011.

[7] J. Zou and Y. Sheng. Research on control technology of dual active full bridge DC-DC converter. *Journal of Physics: Conference Series*, 2030:012011, 2021. doi:10.1088/1742-6596/2030/1/012011.

[8] STM32F303x6 center-aligned PWM ADC timing HAL, 2021. URL: https://stackoverflow.com/questions/46241956/stm32f303x6-center-aligned-pwm-adc-timing-hal.

[9] How to view center-aligned PWM on an oscilloscope, 2021. URL: https://electronics.stackexchange.com/questions/418941/how-to-view-center-aligned-pwm-on-an-oscilloscope.

[10] BP. BP Statistical Review of World Energy 2021, 2021. URL: https://www.bp.com/content/dam/bp/business-sites/en/global/corporate/pdfs/energyeconomics/statistical-review/bp-stats-review-2022-full-report.pdf.

[11] Intergovernmental Panel on Climate Change. Special report on renewable energy sources and climate change mitigation, 2011. URL: https://www.ipcc.ch/report/renewable-energy-sources-and-climate-change-mitigation/.

[12] European Environment Agency. Report on Transport and Environment, 2018. URL: https://www.transportenvironment.org/annual-report-2018/documents/TE-Annual-Report-2018.pdf.

[13] Ministério do Ambiente e da Ação Climática. Roteiro para a neutralidade carbónica 2050: Roteiro da estratégia nacional de longo prazo 2020-2050 [roadmap for carbon neutrality 2050: Roadmap for the national long-term strategy 2020-2050]. https://www.portugal.gov.pt/download-ficheiros/ficheiro.aspx?v=5e5cf276-ef0c-4aa5-bd1c-9c9af23979b5, 2020.

[14] L. Friedman. Biden's electric vehicle goal: 50 percent of sales by 2030. *The New York Times*, 2021. URL: https://www.nytimes.com/2021/08/05/briefing/electric-vehicles-president-biden-climate.html.

[15] C. Argue. EV battery health: How to extend electric vehicle battery life, 2021. URL: https://www.geotab.com/blog/ev-battery-health/.

[16] J. Smith. The different levels of EV charging. *Forbes*, 2022. URL: https://www.forbes.com/wheels/advice/ev-charging-levels/.

[17] Power Sonic Corporation. Levels of EV charging: An overview, 2021. URL: https://www.power-sonic.com/blog/levels-of-ev-charging/.

[18] W. Kempton and S. E. Letendre. Electric vehicles as a new power source for electric utilities. *Transportation Research Part D: Transport and Environment*, 2(3):157–175, 1997. doi:10.1016/S1361-9209(97)00001-1.

[19] D. Lauinger, F. Vuille, and D. Kuhn. A review of the state of research on vehicle-to-grid (V2G): Progress and barriers to deployment. In *Proceedings of the European Battery, Hybrid and Fuel Cell Electric Vehicle Congress*, pages 1–8, Geneva, Switzerland, 2017.

[20] T.-H. Jin, H. Park, M. Chung, K.-Y. Shin, A. Foley, and L. Cipcigan. Review of virtual power plant applications for power system management and vehicle-to-grid market development. *Trans. Korean Inst. Electr. Eng.*, 65(12):2251–2261, 2016. doi:10.5370/KIEE.2016.65.12.2251.

[21] T. Lehtola and A. Zahedi. Electric vehicle to grid for power regulation: A review. In *2016 IEEE International Conference on Power System*, Wollongong, NSW, Australia, 2016. IEEE. doi:10.1109/POWERCON.2016.7753880.

[22] Repsol. Quantos kwh consome uma família. https://www.repsol.pt/particulares/assessoramento/quantos-kwh-consome-uma-familia/.

[23] S. A. Gorji, M. Ektesabi, and J. Zheng. Isolated switched-boost push–pull DC–DC converter for step-up applications. *IET Electronics Letters*, 53(3):177–179, 2017. doi:10.1049/el.2016.4151.

[24] A. A. Aboulnaga and A. Emadi. Performance evaluation of the isolated bidirectional Cuk converter with integrated magnetics. In *Proc. IEEE APEC*, volume 2, pages 1557–1562, Aachen, Germany, Feb. 2004. doi:10.1109/PESC.2004.1355657.

[25] Gustavo G. Koch, Samuel S. Queiroz, Cassiano Rech, Ricardo C. L. F. Oliveira, Renato A. Borges, Eduardo S. Tognetti, and Vinícius F. Montagner. Design of a robust pi controller for a dual active bridge converter. In *2016 12th IEEE International Conference on Industry Applications (INDUSCON)*, pages 1–6, 2016. doi:10.1109/INDUSCON.2016.7874503.

[26] S. Talbi, A. M. Mabwe, and A. E. Hajjaji. Control of a bidirectional dual active bridge converter for charge and discharge of a Li-ion battery. In *Proc. IEEE IECON*, pages 849–856, Yokohama, Japan, Nov. 2015. doi:10.1109/IECON.2015.7392205.

[27] F. Krismer and J. W. Kolar. Accurate small-signal model for the digital control of an automotive bidirectional dual active bridge. *IEEE Transactions on Power Electronics*, 24(12):2756–2768, Dec. 2009. doi:10.1109/TPEL.2009.2027904.

[28] S. Shao, L. Chen, Z. Shan, F. Gao, H. Chen, D. Sha, and T. Dragicevic. Modeling and advanced control of dual-active-bridge dc–dc converters: A review. *IEEE Access*, 7:108280–108305, 2019. doi:10.1109/TPEL.2021.3108157.

[29] S. Q. Zhao, W. Liu, and Y. Sun. Overview of dual-active-bridge isolated bidirectional DC-DC converter for high-frequency-link power-conversion system. *IEEE Transactions on Power Electronics*, Aug. 2014. doi:10.1109/TPEL.2013.2289913.

[30] Haihua Zhou, Tran Duong, Siew Tuck Sing, and Ashwin M. Khambadkone. Interleaved bi-directional dual active bridge dc-dc converter for interfacing ultracapacitor in micro-grid application. In *2010 IEEE International Symposium on Industrial Electronics*, pages 2229–2234, 2010. doi:10.1109/ISIE.2010.5636841.

[31] W. Liu, T. Placke, and K.T. Chau. Overview of batteries and battery management for electric vehicles. *Energy Reports*, 8:4058–4084, 2022. doi:10.1016/j.egyr.2022.03.016.

[32] Infineon Technologies. FF300R12KS4 datasheet. https://pdf1.alldatasheet.com/datasheet-pdf/view/416949/INFINEON/FF300R12KS4.html.

[33] Infineon Technologies. FF400R06KE3 datasheet. https://www.infineon.com/cms/en/product/power/igbt/igbt-modules/ff400r06ke3/.

[34] Philips. CD4050 hex buffer non-inverter IC datasheet. https://components101.com/ics/cd4050-hex-buffer-non-inverter-ic-datasheet-pinout-features.

[35] Semikron. Sk25gh063 datasheet. https://datasheetspdf.com/pdf-file/713580/Semikron/SK25GH063/1.

[36] BK Precision. Bk precision 8500 series programmable DC electronic loads. https://www.bkprecision.com/products/vids/8500.

[37] Zhe Zhang and Michael Andersen. High frequency ac inductor analysis and design for dual active bridge (dab) converters. 03 2016. doi:10.1109/APEC.2016.7468006.

[38] Shuvankar Dey, Surja Sekhar Chakraborty, Saurabh Singh, and Kamalesh Hatua. Design of high frequency transformer for a dual active bridge (dab) converter. In *2022 IEEE Global Conference on Computing, Power and Communication Technologies (GlobConPT)*, pages 1–6, 2022. doi:10.1109/GlobConPT57482.2022.9938249.